REVIEW

Check for updates

The effect of deposition conditions on the properties of Zr-carbide, Zr-nitride and Zr-carbonitride coatings – a review

Anwar Ul-Hamid [ID]

Zirconium-based coatings exhibit a range of useful properties such as high hardness, high temperature stability, biocompatibility, and good resistance to wear, erosion, corrosion and oxidation, making them suitable candidates for use in tribological, biomedical, corrosion-resistant, nuclear fuel, electrical and decorative applications. Common deposition methods reported for Zr-based coatings include cathodic vapor deposition, plasma enhanced chemical vapor deposition, magnetron sputtering, reactive sputtering, reactive melt infiltration, laser pulse deposition, *etc.* Both single and multilayered coatings are produced. This paper presents a review of the effects of deposition methods and operational conditions on the properties of zirconium carbide, zirconium nitride and zirconium carbonitride hard coatings. It describes the role of various process parameters used during the deposition of advanced functional coatings. The present study will contribute to the understanding of hard coatings in general.

1. Introduction

Zirconium, first reported by Martin Heinrich Klaproth in 1789 and isolated by Jöns Jacob Berzelius in 1824, is found in baddeleyite and ores like zircons. Reportedly, the name zirconium is of Persian origin, with "zar"-"gûn" meaning golden in color. Zirconium exists in nature in the form of one long radioisotope and four stable isotopes (^{96}Zr). Since the times of ancient Egypt, a popular zirconium based ore, zircon ($ZrSiO_4$) has been known for purposes including ceramic opacification, foundry works, refractories, *etc.* Over time, zirconium has become more important in corrosion resistant piping, cladding in the nuclear industry, fuel cells, solid electrolytes in oxygen sensors, *etc.* These applications were made possible due to the various important properties of zirconium including its high temperature ionic conductivity, corrosion resistance, good wear resistance, elevated fracture toughness, and high hardness and strength. Zirconium has a high thermal expansion and modulus of elasticity, comparing well with those of iron and steel, respectively. These properties, amongst others, have made zirconium based materials suitable for use in protective coatings for mechanical, chemical and biomedical applications.[1]

Clifton and Johnson[2] patented a method for preparing ZrC fibers in 1968 by reacting carbon with Zr-oxide fibers. The developed product had a higher melting temperature compared to the zirconium oxide fibers in use at the time. ZrC fibers

Center for Engineering Research, Research Institute, King Fahd University of Petroleum & Minerals, Dhahran 31261, Saudi Arabia. E-mail: anwar@kfupm.edu.sa

exhibited lower thermal conductivity and were stable within the operational temperature range. The application of ZrC as a coating on carbon fibers was first reported by Killin *et al.* in 1975.[3] His group evaluated the oxidation resistance of ZrC-coated carbon fibers. In the same year, tungsten fibers were coated with ZrC using a flow-type quartz reactor by Samoilenko and Pereselentseva.[4] Such fibers were used as reinforcement in metal matrix composites such as Ni- and Co-based alloys.

Another novel application reported by Reynolds *et al.* in 1975–1976 consisted of vapor deposition of ZrC coatings on fuel particles to improve the latter's irradiation behavior in a high temperature gas-cooled nuclear reactor.[5,6] It was observed that the coatings successfully retained the fission products. ZrC was selected due to its high melting temperature, reduced tendency to form low-melting-point phases and relatively low neutron-absorption cross-section. ZrC exhibits higher temperature stability than SiC-coated tri-structural isotropic (TRISO) fuel particles. After Reynolds' initial work, research groups in Japan have worked towards developing this technology further in the subsequent decades.[7–14] In addition, contributions to this field from researchers working in the United States,[15–17] France[18] and China[19–22] are also reported in the literature.

In the 1990s, coatings of Ti-based carbides and nitrides were increasingly being used to protect cutting tools. Although similar studies on ZrC were comparatively limited, its characteristics such as high melting temperature, hardness, and corrosion and wear resistance established it as a potential candidate for use in tribological applications. In 1993, reactive magnetron sputtered ZrC coatings with high concentrations of

carbon were reported to exhibit hardness values as high as 5000 HV.[23] Vacuum plasma sprayed coatings exhibited 1600 HV microhardness.[24] Various studies that evaluated the tribological properties of ZrC form part of the related literature.[25–29]

A ZrC coating was identified as a potential candidate to protect components in high temperature environments.[30] Due to its low work function (3.5 eV), it was used as a coating on field emitters to improve the emission stability of field emission scanning electron microscopes.[31] ZrC was successfully coated on roller contacts using a physical vapor deposition technique in 2004.[32] A hardness and a Young's modulus of 1500 HV and 200 GPa were recorded for these coatings. ZrC coatings were also employed in rolling contacts due to their high slip-rolling resistance.[33] ZrC coatings were also evaluated for biomedical applications such as in improving the corrosion resistance and hemocompatibility of implant materials, e.g., SS316L[34] and Ti.[35] They were also used to improve the biological safety of biomedical NiTi shape memory alloys.[36,37] Due to its high electrical conductivity and chemical inertness, potential use of ZrC in sliding electrical contacts such as brushes, microelectromechanical devices, circuit breakers and motor vehicle starters has been suggested.[38]

Various synthesis methods reported for ZrC include cathodic vapor deposition (CVD),[39] magnetron sputtering,[40] reactive melt infiltration,[41] reactive sputtering[42] and PECVD-PIP.[43] Laser pulse deposition has also been employed to produce single-layered ZrC[44,45] and multilayered ZrC/TiN[46] and ZrC/ZrN[47] coatings with reported hardnesses of above 40 GPa.

The potential of sintered ZrN materials for use in machine tools had been recognized from 1960 through the 1970s.[48–51] Zabolotskii et al. coated carbon fibers with ZrN in 1977.[52] Zirconium nitride was studied as a metal coating in 1977 by Caillet et al.[53] In this study, the oxidation kinetics of the coating was determined. Sputtered ZrN was identified as a wear resistant coating material for tribological applications as well as a barrier material for integrated circuit processing in the early 1980s.[54–58] Derradji and Kassabji used a plasma spray method to produce ZrN coatings for possible use in tool applications in 1986.[59] Valikhani and Chandrashekhar[60] compared the performances of twist drills coated with ZrN and TiN in 1987 with the conclusion that the ZrN outperformed the TiN in terms of service lifetime and the quality of drilling. The erosion behavior of ZrN coatings was studied by Sue et al. in 1988[61] and 1990.[62] Various studies were conducted on ZrN coatings in the following two decades to evaluate their erosion protection for turbine and compressor blades,[63,64] microhardness,[65–67] adhesion,[65] wear at 500–600 °C,[68] biocompatibility,[69] orientation dependence,[70] optical and electrical properties,[71] tribology,[72] nuclear fuel element compatibility,[73] and composition and bonding.[74]

From 2011 onwards, investigation into Zr-nitride has continued with various aspects under study including hardness, orientation and phase transition,[75] erosion,[76] microstructure and corrosion,[77] tribology,[78] the colors of coatings,[79] the influence of synthesis parameters,[80–82] adhesion and wear,[83] the influence of yttrium on microstructure and mechanical properties,[84] diffusion barrier properties for nuclear fuel applications,[85,86] the bio- and

cyto-compatibility of human body implants,[87–92] optical, electrical and electronic properties,[93–96] oxidation[97] and modeling and computational analysis.[98–100]

Use of Zr-carbonitride as a coating was first reported by Sintsova and Kbzlovskii in 1970.[101] It was stated that a Zr-carbonitride coating served to increase the corrosion resistance of a steel substrate while retaining the latter's strength. In 1978, Caillet et al. studied the oxidation kinetics of Zr deposited with Zr-carbonitride coatings.[102] Berndt et al. used a CVD technique to synthesize Zr-carbonitride films in 1995 and study their composition, crystallinity and morphology.[103] Manier et al. evaluated Zr-carbonitride coatings for slip rolling resistance in 2010.[33] Various investigations on Zr-carbonitride coatings were undertaken in recent years to study their synthesis parameters,[104] characterization,[105] and optical[106] and biomedical applications.[107–114]

This study presents a review of zirconium carbide, zirconium nitride and zirconium carbonitride hard coatings used for various applications. This paper highlights various methods used for the deposition of these coatings and describes the effects of synthesis parameters on the structure and quality of coatings. The words 'coating' and 'film' are used interchangeably in this paper.

2. Deposition of Zr-carbide, Zr-nitride and Zr-carbonitride coatings

Quite a handful of methods exist for deposition of hard coatings of zirconium nitrides, zirconium carbides and zirconium carbonitrides. Popular amongst the reported techniques are chemical vapor deposition (CVD), physical vapor deposition (PVD), cathodic arc deposition, plasma spray, ion beam implantation and pulsed laser deposition. Various techniques are summarized below. Moreover, the effects of deposition methods and process parameters on the properties of coatings are described in the following sections.

2.1 Methods of coating deposition

2.1.1. Magnetron sputtering deposition. The sputtering technique, as illustrated in Fig. 1, is a physical vapor deposition method that involves pushing materials from a source known as a target to the surface of a substrate. During sputtering, particles ejected from the target possess an energy of up to 100 000 kV; however, only a small proportion (∼1%) of them are ionized. The energized ions shoot in straight lines to impinge on the substrate, causing re-emission of the already deposited materials from the surface of the substrate, i.e. re-sputtering. Another way by which sputtering is achieved is by allowing ions from the target to collide with gaseous atoms at high pressure, thereby moderating the motion of the ions, causing them to diffuse towards the substrate and condense on the surface of the substrate. The impact energy of the ions in the gaseous case depends on the gas pressure and can be modified by changing the latter. The typical gases used are inert with similar atomic weight to the target. Amongst the
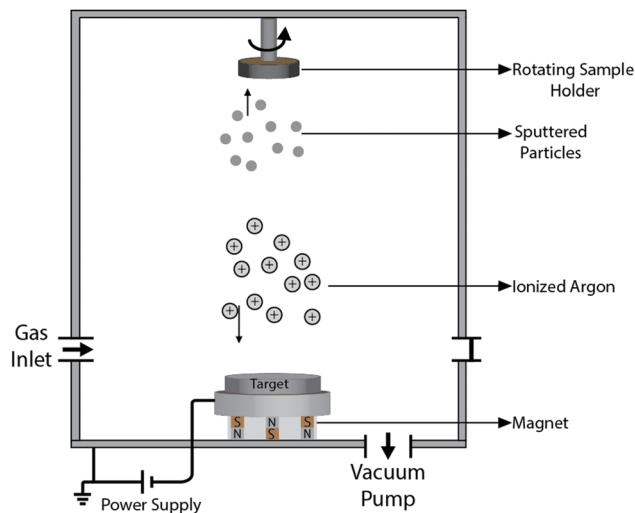
Fig. 1 Schematic illustration of a magnetron sputtering method.

Fig. 2 Ion beam deposition set up with a mass spectrometer.

reported sputtering methods are RF reactive magnetic sputtering,[115] DC/RF reactive magnetron sputtering,[116] DC reactive magnetron sputtering,[117–120] ion beam sputtering,[121] and dual ion beam sputtering.[122]

2.1.2. Cathodic arc deposition method. The cathodic arc deposition method, also known as Arc-PVD, dates back between 1960 and 1970 in the Soviet Union. It is a physical vapor deposition method by which materials are coated through electrolysis vaporization of materials from the surfaces of targets acting as cathodes and deposition by condensation on the substrate. The cathode spot is mobile as it self-extinguishes after some time and reignites in localized spots to initiate the ignition spots. Electromagnetic fields are also used to control the rates of arc movement in case of targets with low melting points. The gas molecules interact with the cathodic arc, leading to their excitation, ionization and dissociation, and hence the formation of compound films.[123] A major disadvantage of the cathodic arc system is that prolonged cathodic spots at any particular location can lead to a large number of badly attached macro-particles of coatings on the substrate. Amongst the reported cathodic arc methods for deposition of ZrC, ZrN and ZrCN coatings are low reflective PVD-arc coating,[124] multilayer coating deposition using a cathodic arc system,[125] monolayer and multilayer TiAlN/ZrN coating deposition using a cathodic-arc evaporation technique using plasma enhanced duct equipment,[126] and non-composite ZrC/amorphous carbon (a-C) deposition on titanium implants using a cathodic-arc evaporation system.[127]

2.1.3. Ion beam deposition. Ion beam deposition (IBD), as illustrated in Fig. 2, is a coating method in which beams of ions are employed to apply materials to the surface of a substrate. An IBD set up is typically made up of a deposition target, ion optics, and an ion source. A mass analyzer can also be incorporated if desired to monitor the species deposited in order to prevent impurities and avoid contamination. The amount of energy applied determines the landing patterns of the ion beams. While low energy enables appropriate landing of
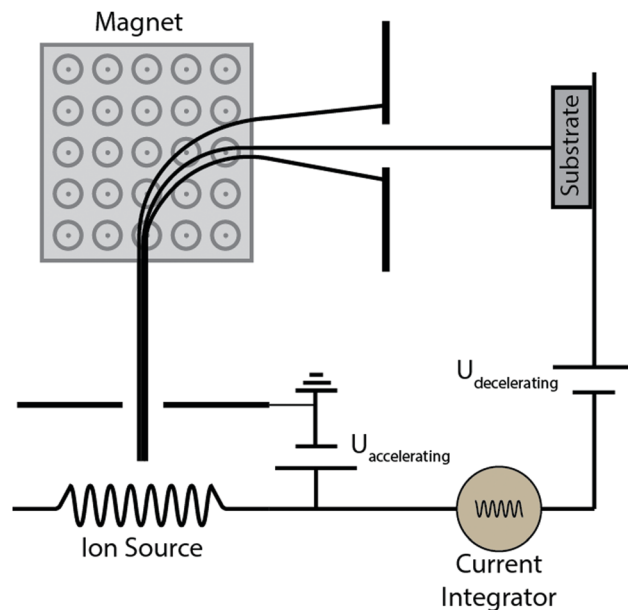
ions on the surface of the substrate, high energy causes implantation of atomic ions into the substrate and fragmentation of molecular ions.

Amongst the reported studies on ion beam deposition methods for ZrC, ZrN and ZrCN coatings are the effect of the methane (CH_4) flow ratio on the micro-nano-structure and hardness of carbo-nitride coatings deposited on AISI 304 stainless steel,[121] ZrCN coatings deposited by a duplex process that combines ion implantation and magnetron sputtering,[104] and epitaxial growth of ZrN/W multilayers using the dual ion beam sputtering (DIBS) deposition method on MgO(001) substrates with bilayer periods of 2.5 nm to 50 nm.[122]

2.1.4. Pulsed laser deposition (PLD). The pulsed laser deposition (PLD) technique, as illustrated in Fig. 3, is a physical vapor deposition technique that involves vaporization of a source (target) through the action of a laser. The source is placed in a vacuum chamber or a chamber filled with specified
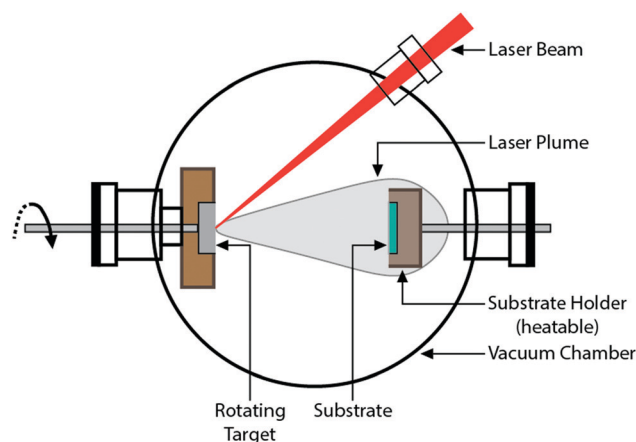

Fig. 3 A configuration for a PLD chamber.

gas (*e.g.* oxygen) while a high-power laser beam is directed on it. The target absorbs the energy which subsequently excites its electrons. Amongst the reported studies on pulsed laser deposition methods for ZrC, ZrN and ZrCN based coatings are the effect of heterogeneous deposition of ZrN coatings using RF-PLD and RPMS with the same bilayer period of 50 nm,[128] and the mechanical properties of ZrC/TiN, ZrC/ZrN and ZrC coatings grown on Si(100) substrates at a temperature of 573 K by pulsed laser deposition (PLD).[129]

2.1.5. Chemical vapor deposition. In chemical vapor deposition (CVD) methods, the substrate (known as wafer) is reacted with volatile components to form deposits on the substrate's surface after which volatile effluents are flushed out by passing gases through the reaction chamber. CVD can be carried out under ultrahigh vacuum (UHVCVD), *i.e.* $< 10^{-6}$ Pa, at low pressure (LPCVD) and at atmospheric pressure (APCVD). Diminished pressure ensures fewer undesirable chemical reactions for better film uniformity across the substrate. Some of the different types of CVD methods are photo-initiated CVD (PICVD), vapor epitaxy, rapid thermal CVD (RTCVD), metalorganic chemical vapor deposition (MOCVD), hybrid physical–chemical vapor deposition (HPCVD), hot filament CVD (HFCVD), combustion chemical vapor deposition (CCVD), atomic layer CVD (ALCVD), remote plasma enhanced CVD (RPECVD), plasma enhanced CVD (PECVD), microwave plasma assisted CVD, direct liquid injection CVD (DLICVD), and aerosol assisted CVD (AACVD). An advantage of CVD methods is that they can produce different forms of deposits including epitaxial, amorphous, polycrystalline and monocrystalline forms. Amongst the reported CVD methods are chemical vapor deposition in a $ZrCl_4$–CH_4–Ar system[130] and medium temperature chemical vapor deposition (MTCVD).[131]

2.1.6. Plasma-enhanced chemical vapor deposition. Plasma-enhanced chemical vapor deposition (PECVD) (Fig. 4) is a popular method that has been used for deposition of zirconium nitrides, zirconium carbides and zirconium carbonitrides. In plasma enhanced or assisted CVD (PECVD or PACVD),

a reacting gas is filled between two electrodes after which AC (RF) or DC is used to ionize the gas molecules usually at low pressure. The ionized gases are called plasma. It is preferred to ionize a lower proportion of the gases in order to create light-weight electrons to maintain high temperature and for better process control. Amongst the reported PACVD methods are pulsed DC PACVD,[132] cathodic-arc evaporation using plasma enhanced duct equipment and pulsed-DC and Radio-Frequency (RF) plasma assisted CVD techniques.[133]

2.1.7. Examples of deposition methods used for Zr-based coatings. Examples of various techniques used for the deposition of a range of Zr-carbide, Zr-nitride, and Zr-carbonitride coatings along with their measured properties are provided in Table 1.

2.1.8. Various gases used in coating deposition. The deposition processes summarized above use high purity argon (99.99%) as the sputtering gas, and nitrogen (N_2, 99.99%) or methane (CH_4) or its mixture as the reactive gas. Nitrogen gas acts as the source for nitride and CH_4 for carbide deposition. A mixture of both is used for carbonitride formation. Occasionally, oxygen gas replaces vacuum in some methods such as laser pulse deposition. The specific carbon to nitrogen concentration ratio required in a coating composition depends on the deposition method and the gas mixture flux and is derived partially by experimentation. Variation in the gas mixture affects the stoichiometry and color of coatings. A larger amount of CH_4 or a smaller amount of nitrogen in the gas mixture results in higher concentration of carbon in the coatings.[136] The substrate bias voltage and temperature also influence the stoichiometry of films. The role of the gas mixture and its flow rate on the coating composition and appearance is described in more detail in the following sections.

2.2. Effect of deposition methods

The method of deposition influences the properties of finished coatings such as their morphology, topography, roughness, and crystallinity. For instance, some finished coatings have a dome-shaped topography; this is typical for coatings produced by PACVD and magnetron sputtering techniques.[135,137] J. Wöhle *et al.*[133] investigated the properties of TiCN and ZrCN coating layers deposited on aluminum by pulsed-DC and Radio-Frequency (RF) plasma assisted CVD techniques at 160 °C. A dome surface topography was recorded for both coating samples. A more homogeneous size distribution of crystals was exhibited by the pulsed-DC plasma deposited coatings, while mixtures of fine and coarse crystal structures were recorded for RF plasma deposited coatings. For both cases, deposition parameters determined the chemical composition of coating layers and the RF plasma permitted wider variation in layer composition. The lower the plasma, the higher the carbon content in the coating layers. Under similar operating conditions, the pulsed-DC plasma technique produced coatings with higher hardness compared to the RF plasma technique. For instance, TiCN layers deposited by RF plasma had a micro-hardness value of 825 HK0.005 as compared to 1800 HK0.005 for the same coating deposited by pulsed-DC. The growth rate
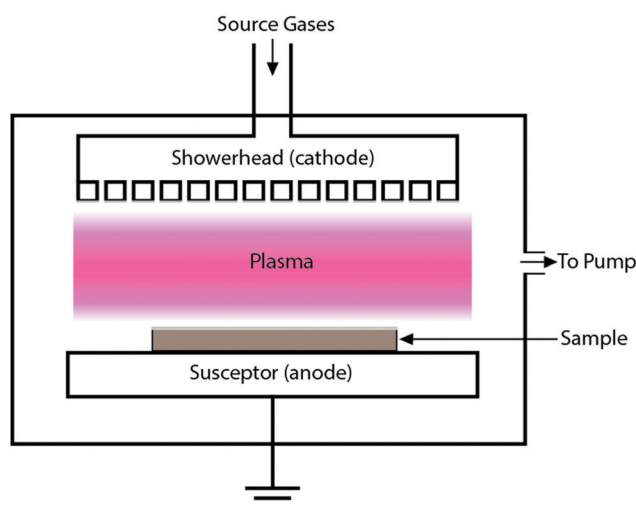

Fig. 4 Schematic illustration of a PECVD technique.

Table 1 Summary of some reported zirconium based (ZrN, ZrC & ZrCN) coatings and their properties

S/N	Ref.	Coating composition	Method of deposition	Properties					
				Hardness	Wear resistance	Corrosion resistance	Friction coefficient	Behaviour with water	Modulus of elasticity
1	Shao-Long et al.[134]	ZrC	Low pressure chemical vapour deposition (CVD)		Mass and linear ablation rates: 0.86–1.1×10^{-4} g s^{-1} and 0.23–0.47×10^{-3} mm s^{-1}, respectively				
2	Ying Long et al.[130]	ZrC and ZrC$_{0.85}$	Chemical vapour deposition (CVD)	ZrC: 24–26.6 GPa, ZrC$_{0.85}$: 21.5–24.1 GPa					ZrC: 303–321 GPa, ZrC$_{0.85}$: 291–313 GPa
3	M. Braic et al.[128]	TiN/ZrN and ZrN/TiN	Deposition by reactive pulsed magnetron sputtering (RPMS) and radiofrequency beam assisted pulsed laser deposition (RF-PLD) on Si and high speed steel	Vickers micro-hardness (HV$_{0.005}$): RM coatings – TiN: 24 GPa, ZrN: 21 GPa, TiZrN: 28 GPa, TiN/ZrN (200/32): 32 GPa, ZrN/TiN (200/32): 30 GPa, ZrN/TiN (10/50): 14 GPa; PL coatings – ZrN/TiN (10/50): 6 GPa					
4	Siao-Fan et al.[125]	CrN/ZrN multilayer coatings	Deposited using a cathodic arc system	Average monolayer coating hardness CrN: 20.3 GPa, ZrN: 21.9 GPa; the maximum multilayer coating hardness (about 28.8 GPa) was achieved with a Cr/Zr atomic ratio of 2.7					Average monolayer coating modulus of elasticity CrN: 228 GPa, ZrN: 267 GPa; the maximum multilayer modulus of elasticity (about 276 GPa) was achieved with a Cr/Zr atomic ratio of 2.7 173.7–326.9 GPa
5	E. Silva et al.[117]	ZrCN	DC reactive magnetron sputtering	10.6–32.4 GPa	Wear rate: 0.38 ± 0.97 to 2.27 ± 0.25 m^3 N^{-1} Lap^{-1} × 10^{15}				
6	K. T. Rie and J. Whole[132]	ZrCN	Pulsed DC PACVD technique; below 200 °C	1400 HK0.01					
7	V. Braic et al.[135]	(Zr, Ti)CN coatings	Magnetron sputtering	25–29 GPa		More electro-positive than an uncoated Ti6Al4V substrate and ZrCN		Hydrophobic; contact angle, 100°	
8	M. Braic et al.[123]	ZrCN and multi-layered Zr/ZrCN	Cathodic method with C45 and M2 steels as substrates	ZrCN: 19.5–28 GPa, Zr/ZrCN: 10.4–21.4 GPa	Scratch test adhesion critical load: ZrCN: 44–54 N, Zr/ZrCN: 74–43 N				
9	M. M. Larijani et al.[121]	ZrN$_{1-x}$C$_X$ where 0 ≤ X ≤ 1	Deposition by an ion beam sputtering method on AISI 304 stainless steel at 400 °C	The maximum hardness was 2520 HV for x = 0.57					
10	E. Grigore et al.[104]	ZrCN	Duplex process that combines ion implantation and magnetron sputtering	The range of the micro-hardness of the coatings obtained was 3180 to 4050 HV0.05. The highest value obtained was with a C/N atomic ratio of 0.9	The highest value of micro-hardness was obtained with a C/N atomic ratio of 0.9 while it exhibited the poorest wear resistance				

Table 1 (continued)

S/N	Ref.	Coating composition	Method of deposition	Properties					
				Hardness	Wear resistance	Corrosion resistance	Friction coefficient	Behaviour with water	Modulus of elasticity
11	M. Braic et al.[118]	(Zr,Nb)CN, (Zr,Ti)CN and (Zr,Hf)CN	Reactive magnetron sputtering technique	ZrCN: 21.4 GPa & 23.6 GPa, (Zr,Nb)CN: 23.1 GPa & 25.4 GPa, (Zr,Ti)CN: 21.4 GPa & 24 GPa and (Zr,Hf)CN: 25.1 GPa & 29.3 GPa			ZrCN: 0.32 & 0.3, (Zr,Nb)CN: 0.32 & 0.27, (Zr,Ti)CN: 0.38 & 0.28, and (Zr,Hf)CN: 0.51 & 0.24		
12	P. Dubey et al.[116]	Zirconium tungsten nitride $(Zr_xW_{1-x}N_y)$	Reactive magnetron sputtering technique	The dual phase (fcc + hcp) film showed maximum hardness (~24 GPa)	The single phase (fcc) film showed maximum (H/Er^2 ~0.2 GPa) and fatigue fracture (H^3/Er^2 ~0.87 GPa)				The dual phase (fcc + hcp) film showed a maximum reduced modulus of elasticity (135 GPa)

of ZrCN layers was about 3.0–4.0 μm per hour on both the Al and Mg alloys, which was twice that of TiCN coatings. The growth rate was attributed to the substrate finish, the type of coating and the constitution of plasma employed during deposition.[137]

Due to lateral variation in plasma energies, the pulse laser deposition technique gives rise to changes in layer thickness across the sample surface. The hardness varies, suggesting that the thickness of each layer in a multilayer system is important. The amount of ablated material during pulse generation plays an important role in achieving a high crystalline quality film.[129]

ZrC coatings were deposited on a SiC-coated graphite substrate using atmospheric (APS) and vacuum plasma spray (VPS) techniques.[29] The formation of ZrO and Zr_2O phases was observed due to the oxidation of ZrC powder in the APS process, giving rise to cracks and pores. On the other hand, the ZrC coating produced through VPS was devoid of oxides and exhibited a denser microstructure, smaller thermal expansion coefficients and higher thermal diffusivity, as compared with the APS-ZrC coating.

Zr-nitride coatings produced using the plasma-enhanced atomic layer deposition (PEALD) technique exhibited the formation of ZrO_2 and/or oxynitride ZrO_xN_y due to ambient surface oxidation.[81] Muneshwar and Cadien that such sputtering artifacts could lead to erroneous conclusions during nanoscale characterization.

Ion beam assisted deposition (IBAD) films show superior performance to other PVD techniques when low process temperatures are required to produce corrosion and wear resistant coatings for materials such as special heat-treated steels and aluminum alloys.[138–143] Films produced using IBAD films possess high structural density and good adhesion. The bulk of the substrate is kept at low temperature during the bombardment of high energy ions.

Plasma sprayed ZrN coatings were produced in a controlled atmosphere.[59] A nitrogen pressure of 700 Torr led to dense deposits with good interlamellar cohesion. The microhardness of the coatings varied between 945 and 1045 HV. At temperatures above 500 °C, oxidation modified the structures of the coatings, rendering them unsuitable for use.

Ion and electron beams from a plasma focus device were used to produce nanocrystalline zirconium carbonitride (ZrCN) coatings on zirconium substrates for multiple (10, 20, 30, 40 and 50) focus shots.[144] Various phases including ZrN, Zr_2N, Zr_3N_4, ZrC and Zr_2CN were detected. The average crystallite size varied from 10 to 20 nm. A microhardness value of 5.6 GPa was observed for ZrCN composite films. The morphology of the coatings was affected by the number of focus shots. An improvement in the crystallinity of the Zr-nitride/carbonitride coatings was observed, which was attributed to the saturation of the residual stresses developed in all planes for higher numbers of focus shots (40–50), in turn caused by enhanced ion induced annealing of the substrate surface.

2.3. Effect of the deposition flow rate

The deposition pressure increases and the deposition rate decreases with an increase in the deposition flow rate of reactive gases during the reactive sputter deposition technique.

At low reactive gas flow rates, the target is cleaned due to the sputtering action, attracting a strong Zr metal flux, leading to high deposition rates. Therefore, at low flow rates the coating is rich in Zr. As the flow rate is increased, poisoning of the target starts to take place, thus increasing the target potential and lowering the deposition rate. The concentration of Zr in the coating decreases, while that of the reactive gas such as nitrogen increases significantly with an increase in the reactive gas flow rate.[82] In addition, the chemistry of the coating depends largely on the composition of the gas mixture and less on the affinity of the gas for Zr. At low flow rates, the coatings formed are dense and large in thickness due to the high deposition rates. The coating morphology is columnar as commonly depicted by coatings deposited with a DC magnetron sputtering method. An increase in the flow rate makes the columnar structure narrower. As the gas flow is increased further, the columnar features start to disappear and are replaced by a dense featureless microstructure.[82] A lower inert gas (*i.e.* argon) flow rate is accompanied by an increased pressure and a decreased target voltage. It results in an increase in Zr content.[82] Reduction in target current also causes an increase in deposition pressure, the extent of which depends on the flow rate of the mixture gas used. The increase in pressure is higher for low gas flow.[82] Increased target current results in Zr-rich coatings.

In another study using a DC magnetron sputtering technique,[79] upon increasing the nitrogen flow rate from zero to 6.0 sccm (the argon rate was fixed at 6 sccm), the phase constitution of the coatings changed from α-Zr, α-ZrN$_{0.28}$, ZrN, and Zr$_3$N$_4$ and finally to an amorphous phase. In another investigation using DC magnetron deposition, single-phase fcc-ZrN was observed at a nitrogen flow rate of up to 1 sccm. From 1 to 6 sccm, ZrN and Zr$_3$N$_4$ phases were detected, while an amorphous phase was identified above 6 sccm due to contamination with oxygen.[80]

Various zirconium nitrides including the metastable phases were deposited by varying the reactive gas composition and energy using dual ion beam sputtering.[145] Use of low energy and a gas (Ar + N$_2$) mixture resulted in the formation of Zr-nitride with metallic properties. High energy and pure nitrogen gas yielded a ZrN$_{1.85}$ transparent insulator (physical properties similar to Zr$_3$N$_4$).

Low reactive gas flow rates (high Zr, low nitrogen) result in silver-colored metallic coatings.[146] An increase in nitrogen to form stoichiometric ZrN imparts a golden color to the coatings.[82,146] Nitrogen rich ZrN$_x$ coatings exhibit dark yellow, brownish yellow, dark brown and finally semi-transparent at N/Zr ratios of 1.2 to 1.3.[146] In another study using DC magnetron sputtering deposition,[79] the color of the coatings changed from silver to dark brown, then to green-yellow and finally to blue with increasing nitrogen flow rate. The golden color was not observed under the experimental conditions used in this study. Stoichiometric ZrN is a thermodynamically stable phase and known to possess a golden color, while Zr$_3$N$_4$ is metastable and mostly transparent.[147] Deposition time affects the coating thickness but has a lower effect on the coating color.

In another study, the DC magnetron sputtering technique was used to study the composition, thickness and hardness of ZrN coatings deposited at different nitrogen partial pressures.[67] Stoichiometric ZrN was formed at a nitrogen partial pressure of 28%. The thickness of the coatings deposited at a constant power decreased with an increase in nitrogen partial pressure. This occurs due to the surface poisoning of the target at higher nitrogen partial pressures, which serves to reduce the sputtering rate. All coatings were golden yellow in color. An increase in nitrogen partial pressure changed the shade from light to dark. Lower N$_2$ partial pressures (7% and 11%) produced a (111) preferred orientation, while high pressures (14% and 28%) gave rise to ZrN with a (200) orientation.

ZrN$_x$ coatings with 200 nm thickness were deposited using RF magnetron sputtering with various nitrogen flow rates.[148] The deposition flow rate decreased significantly from 0.34 to 0.1 nm s^{-1} between nitrogen flow rates of zero and 0.75 sccm. Any further decrease at high flow rates up to 10 sccm was negligible as seen in Fig. 5. The deposition rate decreased once a nitride layer formed at the surface of the Zr target. The sputtering yield of Zr was substantially higher than that of ZrN. The deposition rate was kept continuously low at higher nitrogen flow rates due to an increase in the system pressure, which served to lower the rate of diffusional mass transfer.[148] The argon flow rate was fixed at 2 sccm, while the nitrogen rate was changed from 0 to 10 sccm during which ZrN films of silver, gold, brown, gray and green colors were produced. At high flow rates beyond the golden color, the aesthetics of the films was reduced and became unappealing for the decorative industry. Within a narrow regime of nitrogen flow from 0 to 0.75 sccm, the color of the film changed from silver, gold to golden brown. At a nitrogen flow rate of 3.5 sccm, the film exhibited a dark gray color. At ≥ 4 sccm nitrogen, the color was green.[148] Dual ion beam sputtered Zr$_3$N$_4$ was reported to exhibit a blue color.[149] The argon flow rate has an inconsequential effect on the color of the film.[150]

As the nitrogen flow rate is increased to 0.5 sccm, gold stoichiometric films of ZrN form with dominant (200) and (111)
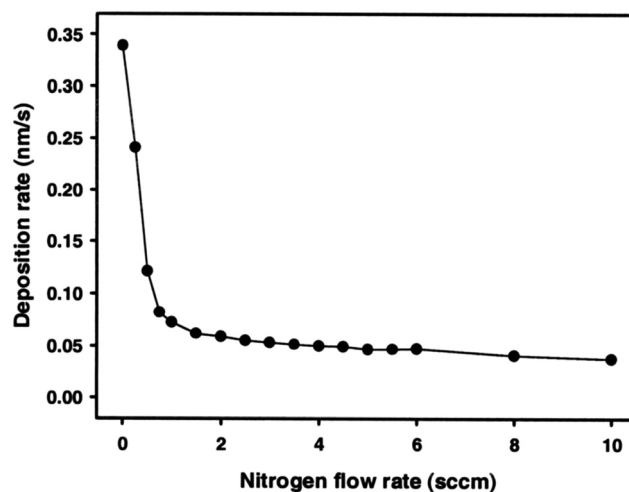

Fig. 5 Deposition rate of ZrN coatings decreases with increasing nitrogen flow rate during the RF sputtering process.[148] (Reproduced with permission from ref. 148.)

peaks along with weak (220) and (311) peaks. As the flow rate increases to 0.75 sccm, the (200) peak becomes stronger still. The surface roughnesses of both films are similar. At 1–3.5 sccm, the intensity of the (200) peak decreases significantly and the (311) peak disappears, while the film becomes grey. With increasing flow rate, the intensities of the (200) and (220) peaks decrease continuously.[148] Simultaneously, the peaks keep shifting to smaller angles and become broadened, indicating the presence of polycrystalline ZrN and the progressive formation of Zr_3N_4.[151,152] As the nitrogen flow increases to 4 sccm, the (200) peak disappears and a broad peak of Zr_3N_4 (320) is formed due to the incorporation of interstitial nitrogen. A continuous increase of nitrogen content forms a Zr_3N_4 phase and makes the structure of the film amorphous.

When the N/Zr atomic ratio is increased from zero to 0.5, the electrical resistivity increases.[146] At these concentrations, nitrogen exists at interstitial sites of the Zr hcp lattice, which introduces grain boundaries and lattice distortion, thus increasing the electrical resistivity. At N/Zr ratios > 0.5, phase transformation to ZrN starts to take place, which serves to decrease the resistivity to the values reported for the cubic ZrN phase. At N/Zr > 1, the electrical resistivity decreases rapidly.

Hollow cathode discharge ion-plating (HCD-IP) was used to deposit nanocrystalline ZrN films on Si(100) and AISI 304 stainless steel substrates.[153] The deposition rate (and the film thickness) was higher for the SS substrate due to its high electrical conductivity. The thicknesses (350 to 550 nm) of the films with a columnar morphology changed with the deposition rate and were not related to the nitrogen flow rate that was varied from 5 to 35 sccm. The N/Zr ratio increased from 0.6 to 0.9 with increasing nitrogen flow rate since a larger number of nitrogen atoms are available in the chamber to react with Zr ions. The roughnesses of the films deposited on the stainless steel substrate were higher compared to those formed on the Si substrate. This was attributed to the higher surface damage caused by ion bombardment to the SS substrate compared to the Si surface at 450 C. Also, the larger substrate current density of the SS surface attracts more ions, resulting in more damage which presents itself as roughness in films.

All samples depicted a (111) preferred orientation.[153] At higher nitrogen flow rates, (200) and (220) peaks appeared. The peak (220) became visible only at a nitrogen flow rate of >25 sccm. The (111) texture coefficient of ZrN decreased slightly for both substrates upon increasing the flow rate. The grain sizes of the ZrN films, measured at 15 to 30 nm, increased with increasing nitrogen flow rate. This could be due to the variation in pressure during deposition as the grain size of the film could be controlled by the mobility of adatoms during growth, which is influenced by the substrate temperature and ion impingement. Coatings yielded fine grain size despite the relatively high substrate temperature (450 °C) used in this study. Ion impingement, on the other hand, increases nucleation sites and decreases grain growth to result in fine grains.

The packing factor of ZrN/Si was observed to increase followed by a decrease, while the packing factor of ZrN/SS 304 first increased and then levelled off,[153] as a result of a change in the flow rate of nitrogen. SS 304 is able to attract a larger number of Zr ions compared to Si. The larger number of Zr ions deliver higher energy and transfer momentum, which increases the mobility of adatoms to form a compact film. A smaller number of Zr ions are attracted by the Si substrate. The increase of the flow rate decreases the energy of the incoming Zr ions such that the adatoms no longer possess sufficient energy to form a dense film.

The hardnesses of the nanocrystalline ZrN films ranged from 23.3 to 26.6 GPa for coatings deposited on both substrates.[153] The residual stress decreased and then increased with nitrogen flow rate. The hardness change was not related to the variation in the nitrogen flow rate or residual stress. Due to the fine grain size, dislocation pile-up or Hall–Petch hardening was not expected. The deformation mechanism of the ZrN films was thought to be grain rotation or grain boundary sliding and not slip by dislocations. In summary, Huang et al. concluded that the nitrogen flow rate changed the N/Zr ratio, packing factor and grain size of the films but had no significant effect on the film thickness, preferred orientation and hardness.

The ZrN films were deposited on polished flat M2 steel substrates by changing the nitrogen pressure and substrate bias voltage using an arc vapor ion deposition process.[154] Dense columnar coatings with their main axis perpendicular to the interface were produced. The coatings became featureless under low pressure and low voltage deposition conditions. The (111) orientation dominated in the ZrN films at low concentrations of nitrogen. At 10 V and 33 μbar, a (200) preferred orientation was produced for coatings that exhibited high nitrogen content. The nitrogen concentration values were not reported in the paper. The changes in the orientation reflected the composition variation.

ZrN films with various stoichiometries were produced using the ion beam assisted deposition method.[95] Stoichiometric ZrN was grown by using N/Zr ratios of 0.98–1.05. The preferred orientation of (111) along with (200) peaks were observed for these films. At N/Zr ratios of 1.1 to 1.26, a (220) preferred orientation was observed. The preferred orientation is influenced by ion bombardment in the high energy range. (220) planes grown parallel to the substrate are known to have low sputtering yields.[155] Under high energy ion bombardment, (220) growth is preferred over the other planes since its re-sputtering rate is comparatively lower. Therefore, the (220) orientation was observed at relatively high N/Zr ratios of 1.1 to 1.26 due to the channeling effect. At a N/Zr ratio of 1.35, crystalline phases disappeared. Nitrogen atoms occupy octahedral sites in a stoichiometric ZrN phase. In over-stoichiometric ZrN, excess nitrogen atoms located randomly in tetrahedral sites result in dilation and amorphization.[156,157]

Thin zirconium nitride films were deposited on Si(100) substrates using ion beam assisted deposition.[74] Arrival rate ratios (ARRs) (N/Zr) of 0.19, 0.39, 0.92, and 1.86 were used. The presence of metal Zr, nitride ZrN, oxide ZrO_2, oxynitride Zr_2N_2O, and carbide ZrC phases was detected in the films. The relative amounts of these compounds were controlled by the ARR (N/Zr). The N/Zr ratio in the film increased with

increasing ARR (N/Zr) until the latter reached 0.92. The excess nitrogen was rejected from the film. Contaminant oxygen and carbon were detected due to the better effect of zirconium.

The mechanical properties of coatings depend on their chemical and phase constitution and structure. Coatings with low nitrogen concentrations show reduced mechanical properties, while well-formed nitrides show superior mechanical properties. Moreover, the presence of an amorphous phase tends to deteriorate the mechanical behavior of the coatings. Dubey et al.[116] evaluated the effect of the amount of nitrogen on the mechanical properties, rate of deposition and structural characteristics of zirconium tungsten nitride ($Zr_xW_{1-x}N_y$) coatings, which strongly depended on pN_2. Film deposition was carried out using a reactive magnetron sputtering technique. Structural, morphological, and cross-sectional analysis and characterization were undertaken using field emission scanning electron microscopy, transmission electron microscopy, shown in Fig. 6, atomic force microscopy, shown in Fig. 7, and grazing angle X-ray diffraction. Elemental composition analysis was carried out using energy dispersion X-ray analysis. It was recorded that for 0.33 Pa $\leq pN_2 \leq$ 0.67 Pa, $Zr_xW_{1-x}N_y$ films showed reflections corresponding to the (fcc + hcp) phase, for 0.20 Pa $\leq pN_2 \leq$ 0.27 Pa, an amorphous phase was obtained, and for 0.07 Pa $\leq pN_2 \leq$ 0.17 Pa, a single (fcc) phase was obtained. Non-monotonic variations of root mean square roughness and reduced film thickness were recorded with increase in pN_2. The dual phase (fcc + hcp) film showed a maximum reduced modulus of elasticity (135 GPa) and hardness ($\sim$24 GPa), while the single phase (fcc) film showed maximum ductility, wear resistance ($H/Er^2 \sim$ 0.2 GPa) and fatigue fracture ($H^3/Er^2 \sim$ 0.87 GPa). High film adhesion to surfaces was exhibited by all film samples and no crack was propagated at a relatively high load of 50 mN.

Silva et al.[117] researched the influence of nitrogen composition on the structural performances of ZrCN coatings with varying compositions of zirconium, nitrogen, carbon and oxygen in order to harness their potential for tribological applications. Nitrogen deposition from 2 to 10 sccm was used with DC reactive magnetron sputtering. The deposition rate of the ZrCN coatings decreased from 2.1 to 1.1 µm h^{-1} with increasing N$_2$ flow due to the progressive poisoning of the targets. At a target potential of −400 V, a deposition rate of 0.7 µm h^{-1} was observed for Zr_xN_{1-x}. For the Zr_xC_{1-x} coatings, an inverse behavior was observed with a higher deposition rate of 1.8 µm h^{-1} and a lower potential of −280 V. The metallic coatings with Zr/(C + N) atomic ratios $\geq$2.9 exhibited a columnar morphology (see Fig. 8a) that is typical for porous coatings grown under low energy ion bombardment, limited adatom mobility and high deposition rates. They exhibited low hardness (13–15 GPa) due to their high Zr content. High coefficients of friction resulted in early failures in tribological tests. For Zr/(C + N) = 1.3, fcc ZrN coatings exhibited a (111) preferred orientation, and a fine-grained dense morphology (see Fig. 8b). The exhibited morphology is due to the decrease in the deposition rate brought about by target poisoning and increasing nitrogen content, which results in a transition from columnar
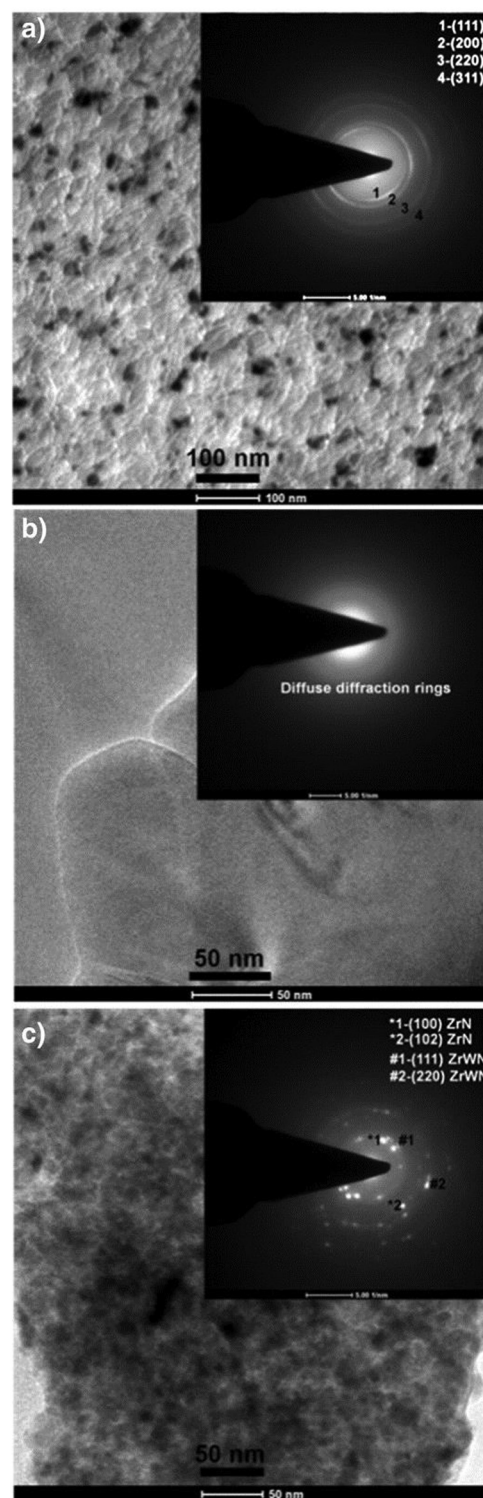

Fig. 6 Selected area diffraction patterns and bright field image topologies of (a) a single fcc phase (0.13 Pa), (b) an amorphous phase (0.27 Pa) and (c) a dual (fcc + hcp) phase (0.47 Pa). (Reprinted from ref. 116 with permission from Elsevier.)

metallic to fine-grained carbonitrides. The XRD peaks broadened and shifted to lower angles due to the C replacement of nitrogen atoms. A ZrCN solid solution phase was formed with
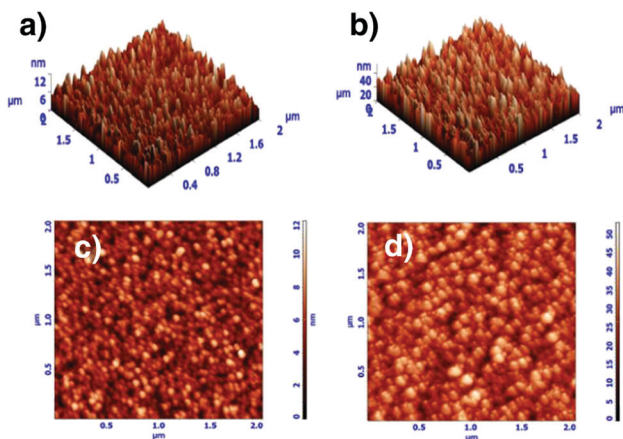
Fig. 7 Atomic force microscope 3D × 2D topological images: (a) and (c) single phase (0.13 Pa) and (b) and (d) dual phase (0.47 Pa). (Reprinted from ref. 116 with permission from Elsevier.)
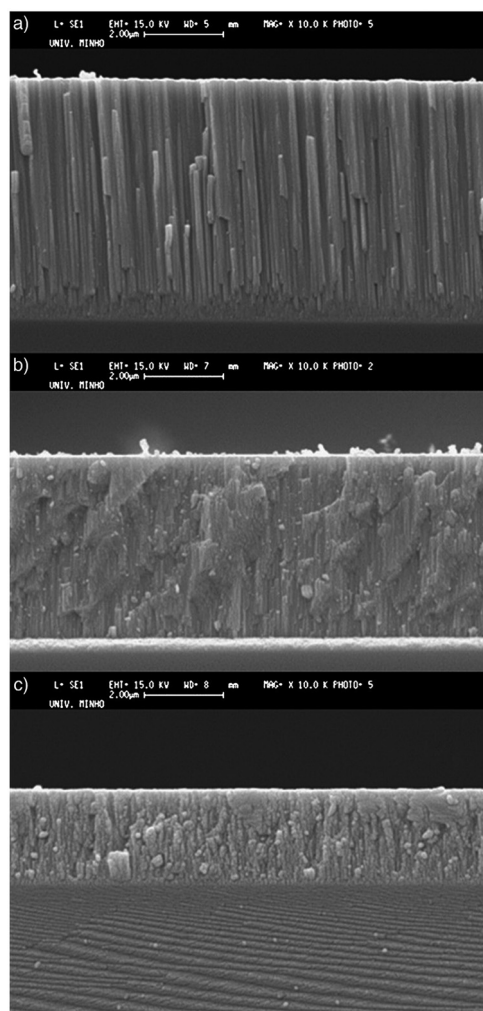

Fig. 8 Various morphologies of Zr-carbonitride films formed at Zr/(C + N) ratios of (a) ≥ 2.9, (b) 1.3 and (c) ≤ 0.7.

hardness values close to 30 GPa. A compact structure resulted for the highest Young's modulus value. For Zr/(C + N) ≤ 0.7,

coatings with a fine-globular morphology (see Fig. 8c) were produced due to the excess carbon and nitrogen that resulted in continuous re-nucleation of grains. The fcc ZrN-type structure was maintained but the (200) orientation became stronger with decreased crystallinity. The hardness was low (9–20 GPa) due to the formation of soft amorphous phases such as a-CN_x and a-C. These phases resulted in low friction.

As per the phase diagram,[158] Zr–C–N can incorporate high amounts of N to form an α-Zr phase, while the C intake is small. Beyond 4 sccm flow of nitrogen, a face centered cubic ZrCN phase which served as a lubricant was formed. The best performance was found in coatings produced with 6 sccm flow of nitrogen with a wear rate of 2.27 ± 0.25 m^3 N^{-1} Lap^{-1} × 10^{15}.

A higher concentration of carbon (due to the increased methane content in the sputtering gas used during the reactive magnetron sputtering process) results in an increased hardness of coatings accompanied by a decrease in adhesion.[23] Higher methane content increased carbon from 1000 to well over 3000 HV. A higher methane content was noted to increase the lattice parameters of the coating, as measured with XRD. This was attributed to the possible incorporation of carbon at interstitial sites in the ZrC lattice.[23] The shift in the XRD peak could also be due to the change in the stress state of the coating due to its increased hardness. He et al.[159] reported a maximum hardness of 31.5 GPa at a Zr/C ratio of 0.97. A further increase in carbon content reduced the hardness.

During the synthesis of Zr based coatings using cathodic arc deposition,[160] it was indicated that the total gas flow rate as well as the $CH_4/(CH_4 + N_2)$ flow rate strongly affected the behavior and properties of the coatings. $CH_4/(CH_4 + N_2)$ ratios of 0.2 to 0.4 gave the highest hardness value (42–45 GPa) as compared to ZrC (19.6 GPa) and ZrN (29.1 GPa).

Varacalle et al.[24] used air plasma spray to produce ZrC coatings. They concluded that a high secondary flow of hydrogen and current during processing resulted in coatings with the highest hardness and thickness, and with the lowest porosity. Various textures of ZrC coatings such as (002), (111)[129] and (111), (220)[23] have been reported. The change in substrate temperature and gas pressure is thought to influence the preferred orientation of the coatings.[23]

Meng et al.[40] reported the structure of ZrC films to consist of nanocrystalline ZrC_x grains embedded in a matrix of amorphous carbon (a-C). For carbon contents above 86 at%, a crystalline ZrC_x phase was not observed. A large amount of a-C resulted in a reduced hardness and an increased resistivity of the film. Concurrently, improvements in the friction coefficient and wear resistance were also observed. Fig. 9 shows the coefficients of friction curves for coatings with various carbon concentrations against Si_3N_4. It can be seen that the friction coefficient decreased upon increasing the carbon content from 44 to 88 at%, which was attributed to the presence of an amorphous carbon phase.

Examination with SEM revealed the wear tracks obtained from the coatings against Si_3N_4 balls after 10 000 laps as shown in Fig. 10. It can be seen that the wear track for the sample with lower carbon content is broader compared to the other, suggesting a loss of the material due to wear.
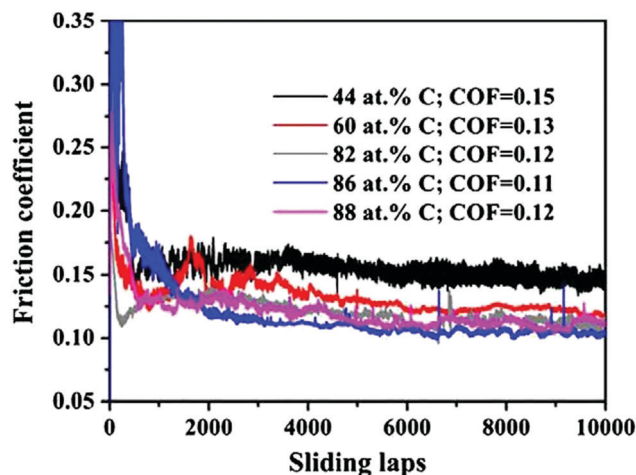
Fig. 9 Friction coefficient curves for coatings with 44–88 at% carbon concentrations against Si_3N_4 balls as a function of sliding cycle. (Reproduced with permission from ref. 40.)
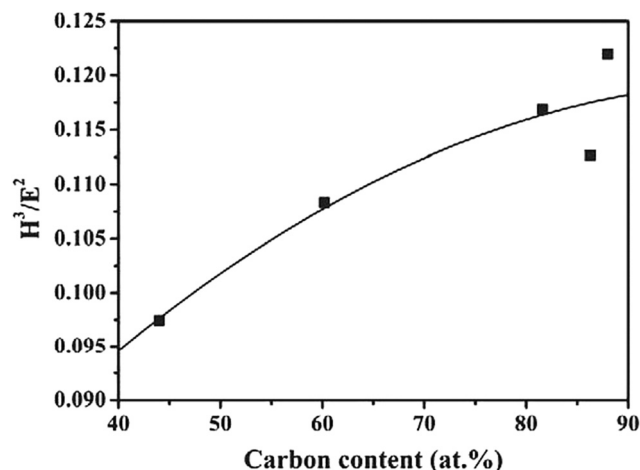

Fig. 11 H^3/E^2 as a function of carbon concentration in the coatings. (Reproduced with permission from ref. 40.)
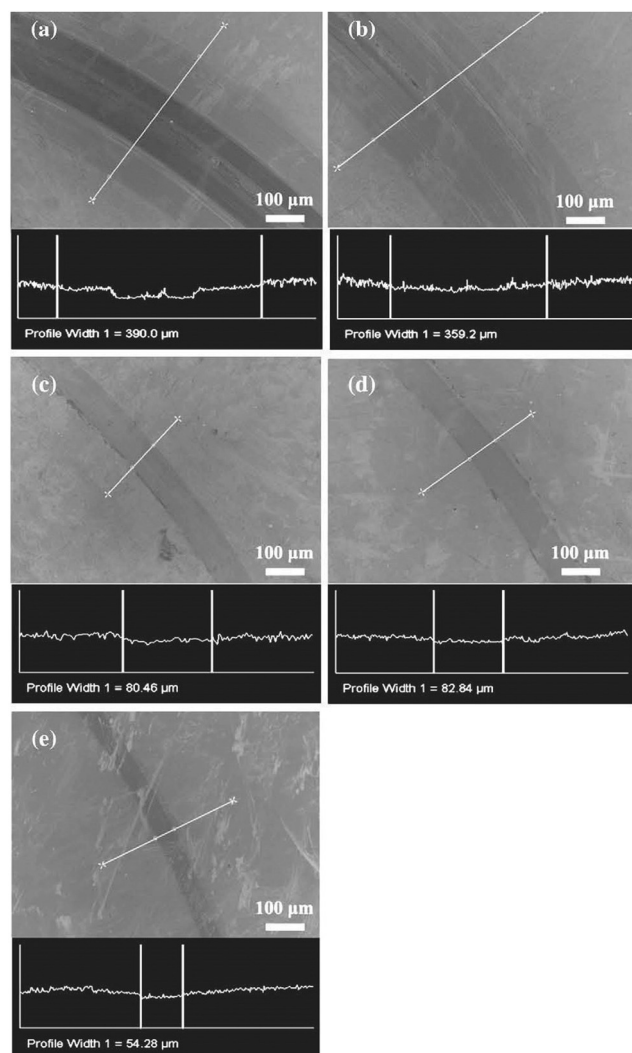

Fig. 10 SEM images of the wear tracks and profiles obtained from coatings with (a) 44, (b) 60, (c) 82, (d) 86 and (e) 88 at% carbon against Si_3N_4 balls after 10 000 laps. (Reproduced with permission from ref. 40.)

Resistance to plastic deformation is defined by the H^3/E^2 ratio. High values of this ratio denote high wear resistance. It can be seen in Fig. 11 that the H^3/E^2 ratio increases with carbon content.

A larger sp^2/sp^3 ratio of the a-C phase relieved stress and improved the electrical properties. The Zr-based films exhibited lower friction coefficients than nanocomposite films based on Ti.

Larijani et al.[121] researched the effect of the methane (CH_4) flow ratio on the micro-nano-structure and hardness of carbonitride coatings deposited on AISI 304 stainless steel by an ion beam sputtering method. Rutherford backscattering, scanning electron microscopy and X-ray diffraction were used to investigate the coatings. The substrate temperature was 400 °C and the working pressure was maintained at 8×10^{-5} Torr. It was shown that an increase in the methane flow ratio changed the crystallographic texture and phase composition of the coating. The crystallographic texture changed from (111) to (220) and the ZrN crystalline phase shifted towards a ZrC crystalline phase via an intermediate phase of $ZrN_{1-x}C_x$, where $0 \leq x \leq 1$. The maximum hardness was 2520 H_v for $x = 0.57$ based on the Vickers hardness test. Bruckner et al.[23] noted that increasing the methane partial pressure changed the structure of the ZrC coating from 'fibrous' to 'open', while the surface was transformed from smooth to flaky. Moreover, increasing the methane content decreased the deposition rate.

Grigore et al.[104] presented ZrCN coatings deposited by a duplex process that combines ion implantation and magnetron sputtering with a view to analyzing the effect of hydrocarbon (butane) and nitrogen reactive flow rates on the morphologies, chemical compositions and structures of coatings under different deposition conditions. For this purpose, glow discharge optical emission spectrometry (GDOES), X-ray diffraction and scanning electron microscopy (SEM) techniques were employed. The range of the microhardnesses of the coatings obtained was 3180 to 4050 HV0.05. A C/N atomic ratio of 0.9 exhibited the highest microhardness but the least wear

resistance values, while the coatings that exhibited the least hardness showed better wear resistance properties.

Craciun et al.[129] researched the mechanical properties of zirconium-based coatings grown by pulsed laser deposition (PLD). ZrC/TiN, ZrC/ZrN and ZrC coatings were grown on Si(100) substrates at a temperature of 573 K by PLD. The cooling rate was 278 K min^{-1}. Auger photoelectron spectroscopy (AES), as shown in Fig. 12, X-ray photoelectron spectroscopy (XPS), X-ray diffraction (XRD), as shown in Fig. 13, and X-ray reflectivity curves were employed for analysis. The results showed that the gas pressure and the nature of the gas used during deposition determined the grain sizes of the deposited crystalline films. The surface morphology and density of the coatings showed marginal improvement when the central part of the laser was used for deposition using an aperture.

ZrC, TiN, and ZrC/TiN multilayer crystalline coatings with a maximum thickness of 400 nm were grown on Si(100) substrates at 300 °C using a pulsed laser deposition (PLD) technique with a KrF excimer laser.[46] The nanoindentation hardness of the multilayers was between 35 and 38 GPa, higher than the 30–33 GPa for single layers of ZrC and TiN. The grain size of the Zr coatings was measured between 8 and 10 nm using XRD and

Fig. 12 AES spectrum acquired from the bulk region (after 5 min sputtering) of the ZrC/ZrN multilayer sample. (Reprinted with permission from ref. 129.)

Fig. 13 Symmetrical XRD (upper traces) and GIXD (lower traces) patterns collected from three different locations on the ZrC/ZrN multilayer sample. (Reprinted with permission from ref. 129.)

TEM. In theory, an inverse Hall–Petch effect is activated for ZrC at or less than 9.4 nm grain size, where the hardness shows a decreasing trend.[161,162] However, such an effect was not observed in this study.

The properties of ZrC/ZrN and ZrC/TiN multilayer structures prepared using pulsed laser deposition were investigated.[47] The use of an Ar atmosphere during deposition resulted in predominantly equiaxed grains in the ZrC/TiN coating with less texture. Under a CH$_4$ atmosphere, a low pressure of 2×10^{-3} Pa produced the best results. It also appeared that the larger thickness of the bilayer produced higher hardness values.

DC unbalanced magnetron sputtering was used to produce ZrCN films with a total flow rate of C$_2$H$_2$ and N$_2$ of 15 sccm.[163] The hardness and wear behavior of δ-Zr(C$_x$N$_{1-x}$)$_{1-y}$ films depended on the variation in the C$_2$H$_2$/N$_2$ ratio.

The film showed a (111) preferred orientation. The film phase, structure and orientation remain unaffected by variations in the C$_2$H$_2$/N$_2$ ratio within the deposition conditions used. The addition of Ti and W caused broadening of ZrCN XRD peaks with no peak shift. New peaks belonging to αW$_2$C, W and TiCN were identified. Additions improved the hardness and wear performance due to the formation of new phases in the film. Ti addition produced better results than W addition. ZrCN, with and without Ti/W additions, showed much better wear performance than TiN.

A combined magnetron sputtering and ion implantation process with nitrogen and hydrocarbon (butane C$_4$H$_{10}$) reactive gases was used to deposit zirconium carbonitride coatings.[104] In this technique, in addition to the DC bias voltage, negative high voltage pulses of 25 Hz were applied periodically to the substrate. High hydrocarbon flow rates resulted in the formation of Zr$_2$CN, Zr$_2$N, ZrC$_{0.6}$ and ZrC. The diffraction lines shifted to lower angles due to the large number of carbon and nitrogen atoms at interstitial positions. The coating grains were columnar with 10–16 μm thickness. Coatings with microhardnesses in the range 3180–4050 HV0.05 were obtained depending on the deposition conditions. These values are higher than those reported for similar coatings produced with magnetron sputtering[163] or those cited for hot pressed carbonitride powders.[164] The wear tests indicated that the coatings with a C/N ratio of 0.9 exhibited the highest microhardness (4050 HV0.05) and their wear resistance was the poorest, while the coatings with a lower microhardness exhibited better wear resistance.

2.4. Effect of the substrate bias voltage

Zr-nitride films were produced at various negative substrate bias voltages that varied from −40 V to −80 V using the cathodic arc ion-plating technique.[165] AISI 304 stainless steel was used as a substrate material. ZrN coatings had a columnar morphology with grain size <15 nm. X-ray diffraction revealed that the texture coefficient of the (111) plane increased with negative bias. The (200) plane has the lowest surface energy in NaCl-type metal nitride films, which, in theory, should show a preferred orientation in this direction. However, kinetic constraints can give rise to other orientations such (111) or (220),
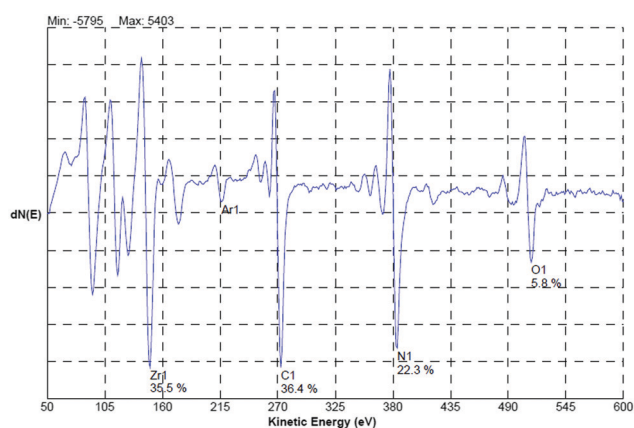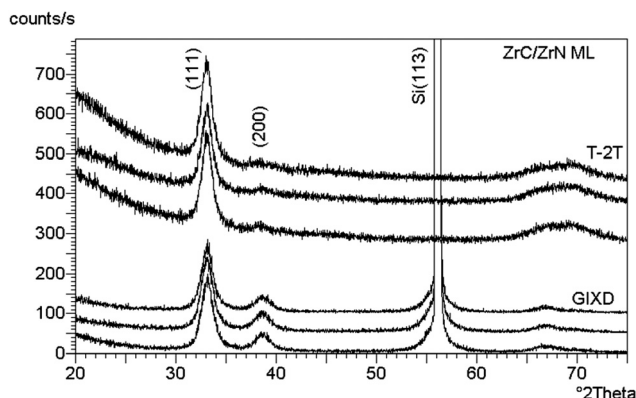
which is attributed to the re-nucleation mechanism proposed by Abadias et al.[166] Large number of defects produced by the bombardment of energetic ions serve as sites for secondary nucleation and grain boundary migration, giving rise to a (111) growth orientation. An increase in bias voltage increases the number of re-nucleation sites, resulting in more grain growth in the (111) orientation. The deposited film specimens were heat-treated at 800 °C for 1 h and the measured grain size was ≤15 nm, i.e. nanoscale grain size.[165] The hardness of ZrN films was studied in terms of their point defects, (111) texture coefficient, and measured crystallinity. It was observed that the hardness of the as-deposited films increased with a decrease in full width at half maximum (FWHM) of the (111) peak and with an increase in the (111) texture coefficient. This observation suggests that highly textured films possessed improved crystallinity and reduced grain boundary mobility. Heat treatment resulted in a decrease in film hardness probably due to the decrease in point defects situated within the films. Heat treatment served to recover point defects as demonstrated by 5.5 GPa reduction in intrinsic residual stress.

Oxygen content in the coatings is influenced by the substrate bias. For DC sputtered ZrN films, the deposition rate decreases monotonically from a positive to negative substrate bias because the deposited species are re-sputtered by energetic argon ions.[146] The nitrogen and oxygen concentrations in the coatings decrease as the positive bias increases. This could be attributed to two reasons. Firstly, at constant power, application of positive bias to the substrate increases the negative bias applied to the target. As a result, a larger number of positive argon ions bombard the target, which leads to increased sputtered Zr atoms in the plasmon. The ionized Zr ions also lose momentum while moving toward the substrate due to an opposing electric field. Secondly, the positive substrate bias attracts more electrons relative to ions toward the substrate, which serves to neutralize nitrogen ions, thus inhibiting the nitride interactions. The electrical resistivity decreases initially and then increases progressively with positive bias as shown in Fig. 14. This is related to the composition change where the

N/Zr ratio decreases to 0.5 for a bias of +50 V, where metastable Zr_2N is observed. An increase in positive bias results in a rapid decrease in the (002) texture due to the higher deposition rate. The oxygen decreases and the nitrogen remains nearly unchanged upon increasing the negative bias. The electrical resistivity decreases linearly with negative bias, which is due to the increase in crystallinity and the decrease in oxygen concentration. The increase in negative bias results in a gentle decrease in the (002) texture.

Zirconium nitride films were deposited on silicon(100) substrates using direct current reactive magnetron sputtering.[75] At a DC negative bias voltage of −26.3 V, a significant (200) preferred orientation in the film was observed. The ZrN diffraction peaks were shifted toward a high angle compared to bulk ZrN, indicating the presence of tensile stress in the film. At a substrate voltage of −80 V, the preferred orientation was (111). The diffraction peaks shifted toward a low angle, indicative of compressive stresses. At −160 V, the (111) preferred orientation became more dominant. At −400 V, the formation of an over-stoichiometric Zr_3N_4 phase was observed. Thermodynamic calculations revealed that high surface energy promotes the (200) orientation, while high strain energy favors the (111) orientation. At a low substrate voltage, the difference in surface energy between (200) and (111) is high (1.85 MPa), while the difference in strain energy is low (0.002 MPa); thus the (200) orientation is preferred. As the voltage is increased from −80 V to −320 V, the difference in the strain energy increases, while the surface energy remains constant, giving rise to a (111) preferred orientation. At −400 V, the strain energy becomes adequately high to drive a phase transition from ZrN to Zr_3N_4. The driving force for the phase transition is considered to be the decrease in strain energy since Zr_3N_4 has lower strain energy than ZrN.

Nanocrystalline ZrN films were deposited on Si(100) and AISI 304 stainless steel substrates using hollow cathode discharge ion-plating (HCD-IP).[167] The ZrN films were close to the stoichiometric composition. The ZrN films deposited on the stainless steel were very smooth, with their roughnesses ranging from 1.1 to 3.9 nm. The columnar structure of the ZrN film became denser with increasing bias. Continuous bombardment of energetic ions serves to peen and compact the film to near bulk density. The presence of a columnar morphology indicates that the energy of ions is not adequate to produce near-bulk compact structures. The width of the columns was 50–100 nm and the length was 250 nm. A cauliflower-like structure was also observed and it was attributed to the low mobility of adatoms and the shadowing effect. Coating thickness was not related to substrate bias.

Zr-nitride films exhibited a (111) preferred orientation on both Si and SS 304 substrates. Zr-nitride films have a strong tendency for a (111) orientation as it is dependent on the atomic mass of the metal in the NaCl-type metal nitride.[168] The ion bombardment of heavy ions such as Zr ions favors (111) growth. It was observed that the FWHM measured in XRD experiments decreased (i.e., the crystalline quality of the ZrN films improved) with increasing bias. The increased negative
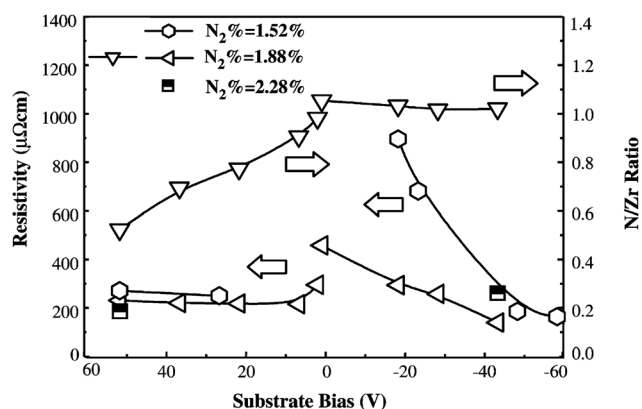

Fig. 14 Influence of the substrate bias (DC power = 150 W) on the resistivity and composition of ZrN$_x$ films. (Reproduced with permission from ref. 146.)

substrate bias results in increased ion bombardment, giving rise to momentum transfer or energy deposition in a certain volume on the surface. This in turn facilitates the movement of adatoms at the surface to equilibrium lattice sites and thus enhance the crystallinity of the film.[169] The hardness values of ZrN films deposited on Si ranged from 27 to 30 GPa, and those on 304 stainless steel were from 32.5 to 40.8 GPa.[168] The substrate bias was not found to have a significant effect on hardness values. The high hardnesses of the films on SS 304 were attributed to the high residual stress in the film, which is due to the large thermal expansion coefficient between the film and the SS substrate. The resistivity is related to the lattice defects in the ZrN film. The resistivity of the ZrN films gradually decreased upon increasing the bias up to −120 V, after which it increased abruptly. The increase in ion bombardment due to the increased bias results in the movement of adatoms to equilibrium sites, increased film compactness and decreased lattice defects. All these factors serve to decrease the resistivity and increase the crystallinity of the film. On the other hand, over-stoichiometric films can show increased resistivity due to the larger density of defects. High energy ions could induce lattice defects too. The abrupt increase observed in the resistivity at high bias voltages could be for the above-stated reasons. The corrosion resistance of ZrN-coated stainless steel in 5% NaCl and 1 N H_2SO_4 + 0.05 M KSCN solutions increased with the bias ranging from 0 to −90 V, then abruptly decreased at −120 V, and then increased again at −150 V. Similar to resistivity, the corrosion behavior was explained by the change in film structure due to bias-induced ion bombardment.[167]

Stoichiometric columnar ZrN films were deposited on Si(100) substrates using the hollow cathode ion-plated (HCD-IP) technique.[170] The thickness of the film was also controlled. The substrate bias was varied from floating to −300 V. The crystallinity improved with increasing negative bias. The ZrN films showed a (111) orientation from 0 to −250 V. At a bias voltage of −300 V, the (220) orientation became the preferred orientation. The change in the orientation was related to the energy delivered to the film. At high ion energy, ion damage or ion channeling of (111) is higher than that of (220) under perpendicular ion bombardment. This results in a change in the preferred orientation from (111) to (220). The hardness values of the ZrN films ranged from 22 to 32 GPa. The films with the (111) preferred orientation are expected to show higher hardness. The active slip systems in ZrN (NaCl-type structure) are of the $\{110\}$ $\langle110\rangle$ family.[171] If the applied force is perpendicular to the (111) plane, the resolved shear stress on all slip systems becomes zero. In this way, the primary slip systems are not activated and thus higher hardness is attained. For films with the (220) preferred orientation, the external force is perpendicular to the (220) plane, and only half of the slip systems have a zero Schmid factor, giving rise to lower hardness values. The packing factor increases with increasing negative substrate bias and reaches a maximum value at bias −50 V, then decreases with increasing negative bias.[170] The increasing bias increases the ion bombardment which results in higher packing density. At increasingly higher bias, the high energy ions introduce defects into the growing film, thereby decreasing the packing density. Similarly, resistivity is also related to lattice defects and follows the same trend as the packing factor. Moreover, a linear relationship was observed between brilliance and the packing factor. At a substrate voltage of −50 V, the ZrN films showed the lowest resistivity of 56 mV cm, the highest packing factor of 0.99, the lowest roughness of 0.66 nm, the highest brilliance of 87.2, and a relatively high hardness of 30.63 GPa.

The dual cathodic arc ion deposition technique was used to grow ZrN on glass and aluminum substrates.[172] The ZrN film prepared at a bias voltage of −100 V was 282 nm in thickness. At −400 V, the measured thickness was 259 nm. The film thickness decreased due to the increased re-sputtering of the deposited film material with increasing negative bias.[173] With a change from −100 V to −400 V, the films became more stoichiometric values (the N/Zr ratio changed from 0.851 to 0.923). At a constant bias of −400 V, as the argon concentration was increased (to $N_2/(Ar + N_2)$ = 15%), the N/Zr ratio decreased significantly to a low value of 0.215. Concurrently, the ZrN film thickness increased from 259 to 351 nm. The marked increase in the growth rate was attributed to the increased yield rate at the target. It was stated that a smaller growth rate at high nitrogen concentrations was due to the lower evaporation rate at the target with nitride formation.

ZrN coatings (3.5 μm in thickness) were deposited on steel and silicon substrates using magnetron sputtering.[71] Application of a bias voltage produced films with a (111) preferred orientation, while (200) growth was observed once the bias was removed. For 0 to −110 V, the lattice constant increased due to nitrogen over-stoichiometry. For negative bias voltages higher than −110 V, the lattice constant decreased due to the preferential re-sputtering of nitrogen. Also, porosities and an increase in film surface roughness were observed due to the re-sputtering phenomenon. The average crystal size was 7 to 9 nm. Unbiased films had 21.8 GPa hardness, which remained unaffected with the variation of the nitrogen and argon flow rates of 3, 4 or 5 sccm and 5, 15 and 25 sccm, respectively. However, at −80 to 90 V, the hardness increased to 27 GPa. The maximum hardness of 39.5 GPa was observed at a bias of −100 V. The hardness decreased to 33 GPa with a further increase in bias. It was stated that at low negative bias the film density increased due to the elimination of voids, which increased the hardness. A further increase in bias induced re-sputtering that reduced the hardness. Compressive stresses were also observed to increase with negative bias.

Application of substrate bias in the reactive magnetron sputtering process increases the target voltage, probably leading to a higher Zr content and a lower nitrogen content in the coatings. It does not, however, cause any variation in deposition pressure, deposition rate and growth mode.[82]

Zr–ZrC–ZrC/DLC gradient composite films were deposited on TiNi alloy using combined plasma immersion ion implantation and deposition (PIIID) and plasma enhanced chemical vapor deposition (PECVD).[28] XPS results indicated that the composition of ZrC depended heavily on the bias voltage. With the increase of bias voltage, the content of ZrC and the sp^3/sp^2
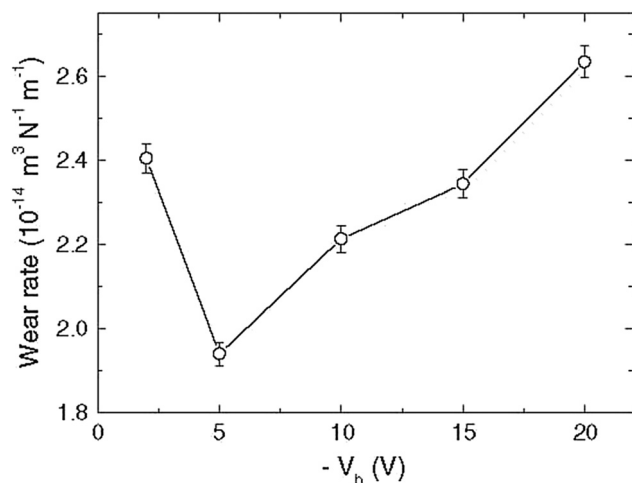
Fig. 15 Plot depicting the wear rate *versus* bias voltage. (Reproduced with permission from ref. 83.)

ratio first increased, reaching a maximum value at 200 V, and then decreased. Similarly, the hardness and elastic modulus of the coatings reached a maximum value of 13 GPa and 200 GPa, respectively, at 200 V, and then decreased gradually until reaching a stable value of 9 GPa and 100 GPa, respectively. The microscratch curve tests showed critical loads of 60 N, which showed that the coatings had excellent adhesion.

RF magnetron sputtering at different bias voltages was used to prepare ZrN films on tungsten carbide substrates.[83] Scratch and ball-on-disk tests were employed to test the adhesion and wear resistance of the coatings. Adhesion to the WC substrate was improved in that the coatings showed higher critical load and scratch hardness along with a lower wear rate at an optimal bias voltage of −5 V when compared to coatings grown with no bias or with higher negative bias voltages (see Fig. 15). Wear tracks formed at the surfaces of samples are shown in Fig. 16. It was concluded that appropriate substrate voltage bias played an important role in the improvement of the tribological properties of the coatings.

2.5. Effect of substrate temperature

During the magnetron sputter deposition process of ZrC films with 200 nm thickness, the growth temperature was varied between 25 and 290 °C. The grain size became larger with temperature except for 290 °C, where the grain structure changed from columnar to nanocrystalline equiaxed due to repeated re-nucleation. The nanoindentation hardness range recorded was 17.5 to 30.2 GPa. The hardness decreased from 25 °C to 180 °C due to stress relaxation and larger grain size then increased again at 290 °C due to smaller grain size, texture strengthening and nanosize effects. The fracture toughness of the film showed exactly the opposite behavior to hardness. The elastic modulus increased from 216.2 GPa to 325 GPa within the temperature range used. The (111)/(200) intensity ratio increased with temperature. At 50–120 °C, the film exhibited the best adhesion characteristics.[25]

ZrC thin films were grown on a silicon(100) substrate using the reactive magnetron sputtering process. The substrate temperature used was from ambient to 500 °C. At less than
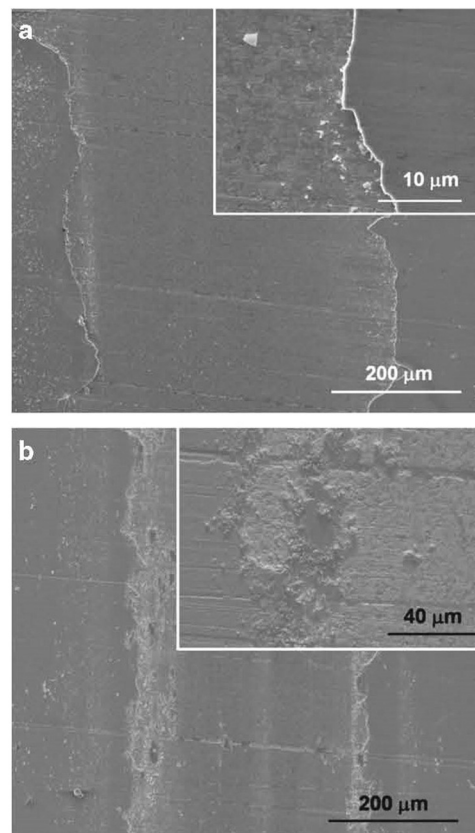

Fig. 16 SEM images of wear tracks formed on samples: (a) ZrN with 10 N load and (b) ZrN with 5 N load. Insets: High magnification images near the track edge. It can be seen that larger loads produced greater material removal. (Reproduced with permission from ref. 83.)

300 °C, ZrC consisted of ZrC nanocrystallites embedded in amorphous carbon, while at higher growth temperatures the films were highly textured. The hardness and elastic modulus increased with temperature with a maximum of 24.8 GPa and 213 GPa, respectively, at 325 °C attributed to the decrease in grain size and the increase in sp^3 bonding compared to sp^2 bonding in ZrC as shown by an XPS study.[42]

Nanocrystalline ZrC coatings with grain sizes from 6 to 20 nm were grown on Si(100) substrates at temperatures from 30 to 500 °C by the pulsed laser deposition technique.[45] The coatings were under compressive residual stress. Nanoindentation hardness values of above 40 GPa were recorded for ZrC coatings prepared at substrate temperatures higher than 300 °C. It was concluded that high hardness values are achieved for highly dense and nanocrystalline coatings.

In another study,[34] ZrC particulates with 5 nm grain size were observed to grow in the (111) preferred orientation at a growth temperature, T_s, of 400 °C. The morphology became smooth as the temperature was increased. It was observed that the growth temperature did not affect the nanoindentation hardness and elastic modulus. Improved adhesion, corrosion resistance and hemocompatibility were recorded for coatings deposited at 200 °C and 400 °C compared with ambient temperature.

Zirconium carbonitride thin films were deposited on steel substrates by means of the dc plasma-assisted chemical vapor deposition technique using metal organic compounds as precursors.[103] At 200 °C the desorption rate was too low to prevent the incorporation of organic fragments in the growing films. Therefore, the metal content of the films remained substoichiometric. The concentrations of oxygen and organic bonded carbon impurities in the films decreased at deposition temperatures above 250 °C. At <300 °C, the films depicted a columnar morphology, a maximum growth rate and a Vickers hardness of 2000 HV. At a substrate temperature of 400 °C or below, dense homogeneous fine grained polycrystalline Zr(C,N) coatings were obtained. At >400 °C, powdery layers were produced due to the decomposition of the precursor in the gaseous phase owing to the low stability of the metal organic compound at elevated temperatures.

Radio-frequency magnetron sputtering was used to produce zirconium carbonitride coatings on AISI 316L austenitic stainless steel.[110] Coatings were almost amorphous at a growth temperature of less than 400 °C, while nanostructured Zr_2CN with a (111) preferred orientation was formed at T_s of 400 °C. This was accompanied by an increase in the nanohardness from 17 GPa to over 32 GPa, an increased elastic modulus and better adhesion. The mobility of adatoms improved at higher T_s and impinging particles with more energy contributed to the formation of a close-packed structure in a state of near thermodynamic equilibrium. Moreover, higher T_s contributed to the reduction in defects while (111) grain texture was formed, resulting in an increase in adhesion.

In another study, Mg- and Al-based alloys were successfully coated with ZrCN and TiCN layers at low substrate temperatures between 110 and 200 °C.[137] The deposition temperature was kept low to avoid reaching the hardening temperatures of these alloys. High substrate temperatures and high bias voltages used along with high C concentrations during the reactive magnetron sputtering process resulted in dense, smooth and hard ZrC coatings.[23] The increased bias voltage decreased the deposition rate, the film structure became denser, and the argon content in the film increased.[23]

The influence of temperature on the chemical and mechanical performances of multi-element (AlCrTaTiZr)N coatings prepared by RF reactive magnetron sputtering was studied by Chia-Han Lai et al.[115] Nitrogen and argon flows were kept constant, while the substrate surface temperature ranged between 100 and 500 °C. X-ray diffraction (XRD) was employed for analysis. Single-phase face-centered-cubic structure was recorded, and the results of analysis showed that the elastic modulus (350 GPa) and hardness (35 GPa) of the researched material were relatively independent of substrate temperature. The elevation in substrate temperature resulted in a monotonic decrease in compressive internal stress from 3.2 to 2.0 GPa; decrease in nitrogen concentration, lattice parameter, and crystallite size; and increase in (200) peak intensity.

The tribological behavior of ZrN coatings deposited on titanium modified austenitic stainless steel (alloy D-9) using the pulsed magnetron sputtering technique at 27–600 °C was

investigated.[78] The ZrN coatings prepared at higher deposition temperature showed lower coefficients of friction.

2.6. Effect of the energy of ions used during synthesis

Abadias et al.[119] used real-time wafer curvature measurements to evaluate stress development during the magnetic sputtering of ZrN thin films and Ti–Zr–N solutions. For a given target, the plasma conditions (M_{Ta} = 180.9, M_{Zr} = 91.2 and Z_{Ti} = 47.9 g mol^{-1}) and the metal target were changed to modify the energy of the incoming ions, backscattered Ar or sputtered atoms. Monte-Carlo simulation was employed for analysis. The stress gradient was recorded under low energy deposition conditions, which was evident from the quick development of compressive stress for all films at the early stages of growth, which eventually reversed to tensile stress as the film thickness increased. Under high energy conditions, compressive stress was predominant even with increase in film thickness because a better microstructure and a smooth surface were recorded. Impingement of ions with high energy and momentum gives rise to a large number of nucleation sites at the substrate surface, resulting in the fine grain size of the coating.[153]

The deposition rate increases with DC power used during the DC magnetron sputtering of ZrN films.[146] The reaction rate of nitrogen with Zr decreases because the number of sputtered Zr atoms increases. The stoichiometry region for the formation of ZrN slightly broadens and moves toward a higher nitrogen flux ratio.

Ion assisted deposition was used to prepare ZrN coatings at various ion beam energies.[174] The optimum growth conditions were an ion energy of 150–200 eV, a N/Zr ratio of 1.2–1.5 and a substrate temperature of 820 °C. ZrN coatings developed using the ion beam assisted deposition technique exhibited (111) and (200) preferred orientations at beam energies of 500 V and 700 V respectively.[70]

2.7. Effect of deposition distance

DC magnetron sputtering was used to deposit ZrN coatings at various deposition distances.[146] The longer the deposition distance, the smaller the deposition rate as the particles arriving at the substrate experience scattering. The interactions between nitrogen and zirconium as well as oxygen impurities increase. The N/Zr atomic ratio increases initially and the oxygen content increases with the deposition distance, which causes an increase in the electrical resistivity of the deposited films. The N/Zr atomic ratio decreases slightly at deposition distances >80 mm probably due to the presence of oxygen in the films, since the Zr–O bond is stronger than the Zr–N bond. The crystallinity degrades with deposition distance.

2.8. Effect of deposition time

The deposition rate in electron-beam evaporation is not a linear function of deposition time. ZrN coatings were prepared using hollow cathode discharge ion-plating.[167] The same duration was used for all samples, but the coating thickness had large variation from 0.47 to 1.17 μm. Nitridation of the Zr source occurs during deposition, which lowers the vapor pressure of Zr

and the deposition rate. Low vapor pressure targets require use of higher temperature or greater power for deposition.

2.9. Effect of coating composition

Braic et al.[135] investigated the protective qualities of hard ZrCN coatings. Different ratios of metal and non-metal components of varying thickness and hardness were evaluated for properties such as corrosion resistance and surface wettability amongst other properties. The coated samples showed better resistance to corrosion compared to Ti-6Al-4V alloy and ZrCN, which may be due to their reduced roughness. Their crystal structures possessed composite structures made up of ZrCN and amorphous C(N) (a-C(N)) and they were hydrophobic with contact angles higher than $100°$.

Chen et al.[125] researched the influence of the chemical concentration ratio (Cr/Z ratio) on the Daimler-Benz Rockwell-C (HRC-DB) adhesion, nanoindentation, microhardness, roughness, wear resistance and scratch resistance of the multilayer CrN/ZrN coatings that were deposited using a cathodic arc system. The Cr/Zn atomic ratio was controlled in the range of 1 to 2.5 by using various values of target current. The phase and concentration of the CrN/ZrN multilayer were analyzed using a glancing angle X-ray diffractometer and a field emission electron probe micro-analyzer (FE-EPMA) respectively. It was shown that the Cr/Zr chemical composition ratio remarkably affected the tribological and hardness performances of CrN/ZrN multilayer coatings. The maximum coating hardness (about 28 GPa) was achieved with a Cr/Zr atomic ratio of 2.1. The occurrences of reflections of the (111), (200), (220) and (311) indices were recorded for ZrN single layer coatings. For CrN/ZrN multilayer coatings, even though some characteristic reflections were seen, different XRD reflection intensities were noticed. In addition to these observations, reflections along the ZrN(111) plane were produced in multilayered thin films.

Braic et al.[118] investigated the effect of adding Nb, Hf and Ti to ZrCN based coatings. Base coats of two different metal ratios were used: highly stoichiometric $((Me_1 + Me_2) \sim 3)$ and quasi-stoichiometric $((C + N)/(Me_1 + Me_2) \sim 1)$ where films are composed of metals Me_1 and Me_2. Coating preparation was undertaken using the reactive magnetron sputtering technique with the aim of investigating their wear resistance, hardness, surface morphology, texture and phase compositions. Nanocomposite structures were observed in the films. The structures consisted of amorphous carbon and crystalline metal carbon nitrides. The quaternary coatings showed better wear resistance and mechanical properties. The lower the metal content, the lower the friction coefficient, the higher the hardness and the finer the morphology. Lower deposition rates were recorded with decrease in metal content. Coatings with equal metal and non-metal ratios exhibited similar Raman spectra. The spectra for metals containing carbon films, carbon nitride, and amorphous carbon were similar and they showed a graphite structure. Increases in the D & G peaks in the Raman analysis were noticed with increase in carbon content for both coating types and for all metals. The friction coefficient μ versus sliding distance of the deposited film is shown in Fig. 17 and it was
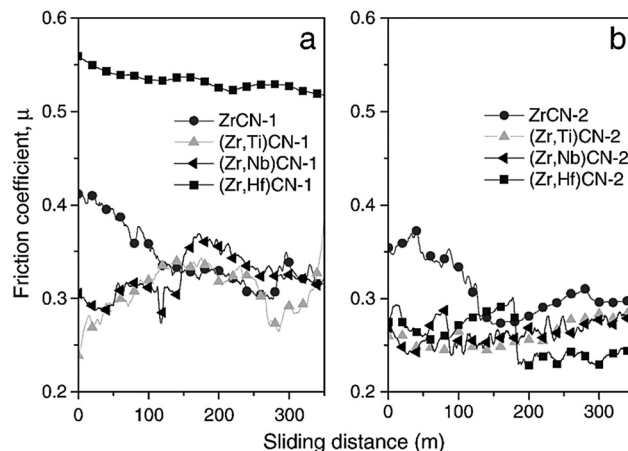

Fig. 17 Friction coefficients (μ) and sliding distances of ZrCN, (Zr,Ti)CN, (Zr,Hf)CN and (Zr,Nb)CN coatings: (a) low non-metal content and (b) high non-metal. (Reprinted from ref. 118 with permission from Elsevier.)

discovered that the films with high concentrations of non-metal showed lower friction coefficients.

Balaceanu et al.[160] evaluated the corrosion resistance, tribological, adhesion, hardness and surface roughness properties, texture, chemical bonding, phase and elemental compositions of super-hard ZrCN based coatings deposited on high speed steel, plain carbon steel and Si substrates by a cathodic arc method. Al and Ti were added to the base coatings to check for their effects on the above properties. Coating characterization was carried out by X-ray diffraction (XRD), GDOES, and XPS techniques, amongst others. The addition of Al and Ti to ZrCN resulted in the improved properties of TiAlCN, ZrCN, ZrC and ZrN based coatings.

Long et al.[130] examined the mechanical properties, microstructure and phase composition of Zr-carbide coatings (ZrC and $ZrC_{0.85}$) deposited by means of chemical vapor deposition. For this purpose, X-ray diffraction (XRD) and X-ray photoelectron spectroscopy (XPS) were used for analysis. Hardnesses of 22–28 GPa and Young's moduli of ~ 303–321 GPa were reported for stoichiometric (ZrC) coatings, which are more than those of non-stoichiometric coatings ($ZrC_{0.85}$). Cubic ZrC was formed and a strong (200) texture normal to the surface of the substrate was exhibited in both coatings. Compared to the stoichiometric ZrC, the peak position corresponding to the (200) reflection in the non-stoichiometric coating ($ZrC_{0.85}$) was closer to the 2Θ value and the lattice parameter was slightly lower. The presence of both Zr and C at the surface of the coating was confirmed with XPS. The binding energies for ZrC and $ZrC_{0.85}$ related to the Zr 3d peak were different, thus confirming the change in stoichiometry within ZrC. Peaks corresponding to oxygen present due to contamination were also observed, confirming the existence of the Zr–O bond (Fig. 18).

3. Conclusions and recommendation

Various deposition methods such as magnetron sputtering, cathodic arc deposition, ion beam deposition, pulsed laser
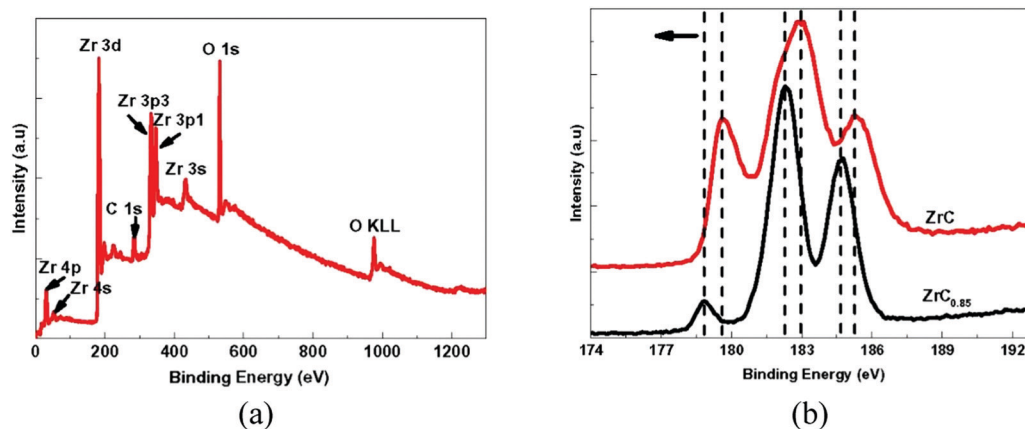
Fig. 18 XPS results obtained from ZrC coatings showing (a) a survey spectrum with peaks representing various energy levels. (b) Variation of intensity at core-levels in stoichiometric ZrC and non-stoichiometric $ZrC_{0.85}$ corresponding to Zr 3d. (Reproduced with permission from ref. 130.)

deposition, and chemical vapor deposition are available for the deposition of Zr-based hard coatings, which have found applications in the mechanical, chemical, nuclear and biomedical sectors. Deposition conditions that largely affect the structure and properties of coatings include the coating composition, reactive gas flow rate, substrate bias and temperature. In addition, the deposition time and distance, ion kinetic energy and coating method also affect the quality of coatings.

At low deposition rates, coatings are columnar and large in thickness. At high rates, coatings become dense and featureless. The chemical constitution of the coatings is heavily influenced by the deposition flow rate of reactive gases such as nitrogen. For instance, as the rate is increased, the phase constitution changes from α-Zr, $α-ZrN_{0.28}$, ZrN, Zr_3N_4 and finally to an amorphous phase.

The hardness of ZrCN coatings is affected by the carbon content and it increases with increase in carbon content and discharge voltage. It was reported that the hardness of ZrCN and Zr/ZrCN films was improved with increasing carbon concentration. A low nitrogen flow rate results in a metallic silver color, while increased nitrogen supply imparts a golden color to the coatings. At high nitrogen partial pressures, the film thickness decreases due to the surface poisoning of the target. The electrical resistivity changes with the flow rate depending on the phase constitution of the coating. The hardness of the coatings also depends on the grain size, structure, defects, preferred orientation, residual stresses and chemical and phase constitution of the coatings. A high Zr content in the coating leads to reduced hardness. The formation of soft amorphous carbon or CN_x exhibits low hardness, friction and high resistivity. Over-stoichiometric films also exhibit higher resistivity. For ZrCN coatings, a C/N ratio of 0.9 gives high hardness. Generally, (111) and (200) preferred orientations are observed for stoichiometric ZrN and over-stoichiometric ZrN, respectively.

An increase in negative bias voltage at the substrate may influence the preferred orientation, phase constitution, hardness and degree of crystallinity. At a low negative voltage, the (200) orientation is preferred. At a high negative voltage, the (111) orientation is preferred. With increasing voltage, the crystallinity increases, the phase changes from ZrN to Zr_3N_4 and the columnar coating structure becomes denser, in turn increasing the hardness. The coating thickness is reduced due to the re-sputtering effect.

The grain size of the Zr-based coating increases with increasing substrate temperature unless repeated re-nucleation occurs. The hardness decreases and the fracture toughness increases as the temperature increases. Better adhesion occurs at temperatures greater than ambient temperature. An increase in substrate temperature results in a decrease in compressive stress, nitrogen concentration, lattice parameters, and crystallite size and an increase in (200) peak intensity in multi-element nitride coatings.

Increased ion energy results in a change in the preferred orientation from (111) to (220) for ZrN. It also favors build-up of compressive stresses. The longer the deposition distance, the smaller the deposition rate. The same duration will give different coating thicknesses due to the poisoning of the source.

Based on existing work, much research needs to be carried out on Zr-based coatings in the areas including cost-effective and easily controlled methods of preparation, energy consumption, condensation challenges in PLD techniques, etc. Likewise, induced porosity, oxidation introduced by the coating processes, altered substrate properties, use of multi-deposition methods, minimization of coating property trade-offs during optimization, and multilayered coatings make interesting topics of research.

Conflicts of interest

There are no conflicts to declare.

Acknowledgements

References

1 M. Hisbergues, S. Vendeville and P. Vendeville, Zirconia: established facts and perspectives for a biomaterial in dental implantology, *J. Biomed. Mater. Res., Part B*, 2009, **88B**(2), 519–529.

2 R. A. Clifton Jr. and R. C. Johnson, Method of preparing zirconium carbide fibers and the product thereof, *US Pat.*, US3385669A, 1968.

3 V. S. Kilin, E. M. Cherednik, L. N. Shcheglova, V. S. Ostrovskii and V. S. Dergunova, Oxidation resistance of carbon fibers with protective coatings, *Poroshk. Metall. (Kuibyshev)*, 1975, **2**(146), 44–47.

4 V. G. Samoilenko and L. N. Pereselentseva, Deposition of zirconium carbide coatings acting as diffusion barriers in composites consisting of a metallic matrix and refractory metal fibers, *Poroshk. Metall. (Kuibyshev)*, 1975, **9**(153), 35–39.

5 G. H. Reynolds and J. L. Kaae, Chemical Vapor Deposition of Isotropic Carbon–Zirconium Carbide Particle Coatings, *J. Nucl. Mater.*, 1975, **56**(2), 239–242.

6 G. Reynolds, J. Janvier, J. Kaae and J. Morlevat, Irradiation behavior of experimental fuel particles containing chemically vapor deposited zirconium carbide coatings, *J. Nucl. Mater.*, 1976, **62**, 9–16.

7 T. Ogawa and K. Ikawa, Crushing strengths of SiC-Triso and ZrC-Triso coated fuel particles, *J. Nucl. Mater.*, 1981, **98**(1–2), 18–26.

8 T. Ogawa and K. Ikawa, *J. Nucl. Mater.*, 1982, **99**, 85.

9 T. Ogawa, K. Ikawa, K. Fukuda, S. Kashimura and K. Iwamoto, Research and development of ZrC-coated UO2 particle fuel at JAERI, *Conference on Nuclear Fuel Performance*, London, 1985.

10 T. Ogawa and K. Ikawa, Reactions of Pd with SiC and ZrC, *High Temp. Sci.*, 1986, **22**, 179–193.

11 T. Ogawa, K. Fukuda, S. Kashimura, T. Tobita, F. Kobayashi, S. Kado, H. Miyanishi and I. T. A. T. Kikuchi, Performance of ZrC-Coated Particle Fuel in Irradiation and Postirradiation Heating Tests, *J. Am. Ceram. Soc.*, 1992, **75**, 2985–2990.

12 T. Ogawa and K. Fukuda, ZrC Coated Particle Fuel Development, *International symposium on advanced nuclear energy research, Mito (Japan)*, 1992, pp. 554–560, https://inis.iaea.org/search/search.aspx?orig_q=RN:25010826.

13 K. Minato, T. Ogawa, K. Fukuda, H. Sekino, I. Kitagawa and N. Mita, Fission product release from ZrC-coated fuel particles during post-irradiation heating at 1800 and 2000 °C, *J. Nucl. Mater.*, 1997, **249**(2–3), 142–149.

14 J. Aihara, S. Ueta, A. Yasuda, H. Takeuchi, Y. Mozumi, K. Sawa and A. Y. Motohashi, Effect of Heat Treatment on TEM Microstructures of Zirconium Carbide Coating Layer

in Fuel Particle for Advanced High Temperature Gas Cooled Reactor, *Mater. Trans.*, 2009, **50**(11), 2631–2636.

15 L. L. Snead, Y. Katoh and S. Kondo, Effects of fast neutron irradiation on zirconium carbide, *J. Nucl. Mater.*, 2010, **399**, 200–207.

16 Y. Katoh, G. Vasudevamurthy, T. Nozawa and L. L. Snead, Properties of zirconium carbide for nuclear fuel applications, *J. Nucl. Mater.*, 2013, **441**, 718–742.

17 G. Vasudevamurthy, Y. Katoh, J. Aihara, K. Sawa and L. Snead, Microstructure and mechanical properties of heat-treated and neutron irradiated TRISO-ZrC coatings, *J. Nucl. Mater.*, 2015, **464**, 245–255.

18 K. Plevacova, C. Journeau, P. Piluso, V. Zhdanov, V. Baklanov and J. Poirier, Zirconium carbide coating for corium experiments related to water-cooled and sodium-cooled reactors, *J. Nucl. Mater.*, 2011, **414**, 23–31.

19 C. Liu, B. Liu, Y. Shao, Z. Li and C. Tang, Preparation and Characterization of Zirconium Carbide Coating on Coated Fuel Particles, *J. Am. Ceram. Soc.*, 2007, **90**(11), 3690–3693.

20 Y. Wang, Q. Liu, J. Liu and L. Z. A. L. Cheng, Deposition Mechanism for Chemical Vapor Deposition of Zirconium Carbide Coatings, *J. Am. Ceram. Soc.*, 2008, **91**(4), 1249–1252.

21 W. Sun, X. Xionga, B. Y. Huang, G. D. Li, H. B. Zhang, P. Xiao and Z. A. X. L. Zheng, Microstructural Control of Zirconium Carbide Coating Prepared by Chemical Vapor Deposition, *ECS Trans.*, 2009, **25**(8), 291–299.

22 X. Geng, F. Yang, H. Liu, X. Lu and P. Xiao, Palladium Migration Through a Zirconium Carbide Coating in TRISO-Coated Fuel Particles, *J. Am. Ceram. Soc.*, 2016, **99**(4), 1455–1463.

23 J. Bruckner and T. Mantyla, Reactive magnetron sputtering of zirconium carbide films using Ar–CH₄ gas mixtures, *Surf. Coat. Technol.*, 1993, **59**, 166–170.

24 D. J. Varacalle, L. B. Lundberg, H. Herman, G. Bancke and W. L. Riggs, Vacuum plasma sprayed zirconium carbide coatings, *Surf. Coat. Technol.*, 1994, **68/69**, 86–91.

25 C.-S. Chen, C.-P. Liu and C.-Y. Tsao, Influence of growth temperature on microstructure and mechanical properties of nanocrystalline zirconium carbide films, *Thin Solid Films*, 2005, **479**(1–2), 130–136.

26 W. H. Kao, Optimized a-C coatings by doping with zirconium for tribological properties and machining performance, *Diamond Relat. Mater.*, 2007, **16**(11), 1896–1904.

27 D. Ferro, J. V. Rau, V. Albertini, A. Generosi, R. Teghil and S. M. Barinov, Pulsed laser deposited hard TiC, ZrC, HfC and TaC films on titanium: hardness and an energy-dispersive X-ray diffraction study, *Surf. Coat. Technol.*, 2008, **202**(8), 1455–1461.

28 Y. F. Zheng, X. L. Liu and H. F. Zhang, Properties of Zr–ZrC–ZrC/DLC gradient films on TiNi alloy by the PIIID technique combined with PECVD, *Surf. Coat. Technol.*, 2008, **202**(13), 3011–3016.

29 C. Hu, X. Ge, Y. Niu, H. Li, L. Huang, X. Zheng and J. Sun, Influence of Oxidation Behavior of Feedstock on Microstructure and Ablation Resistance of Plasma-Sprayed
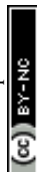
Zirconium Carbide Coating, *J. Therm. Spray Technol.*, 2015, **24**(7), 1302.

30 F. M. Charbonnier, *J. Vac. Sci. Technol., B*, 1998, **16**(2), 880.

31 F. Charbonnier, W. Mackie, T. Xie and P. Davis, *Ultramicroscopy*, 1999, **79**, 73.

32 M. Kuhn, P. W. Gold and J. Loos, Wear and friction characteristics of PVD-coated roller bearings, *Surf. Coat. Technol.*, 2004, **177–178**, 469–476.

33 C.-A. Manier, H. Ziegeleb, J. Barrigac, J. Goikoetxeac and M. Woydt, Zirconium-based coatings in highly stressed rolling contacts as alternative solution to DLC and ta-C coatings, *Wear*, 2010, **269**, 770–781.

34 D. Ming-hui, Z. Hong-Sen, Z. Chi and J. Xing, Characterization of ZrC coatings deposited on biomedical 316L stainless steel by magnetron sputtering method, *Surf. Coat. Technol.*, 2013, **224**, 34–41.

35 L. Floroian, D. Craciun, G. Socol, G. Dorcioman, M. Socol, M. Badea and V. Craciun, Titanium implants' surface functionalization by pulsed laser deposition of TiN, ZrC and ZrN hard films, *Appl. Surf. Sci.*, 2017, **417**, 175–182.

36 T. Duerig, A. Pelton and D. Stockel, An overview of nitinol medical applications, *Mater. Sci. Eng., A*, 1999, **273–275**, 149–160.

37 C. Chu, H. Ji, L. Yin, Y. Pu, P. Lin and P. K. Chu, Fabrication, properties, and cytocompatibility of ZrC film on electropolished NiTi shape memory alloy, *Mater. Sci. Eng., C*, 2011, **31**, 423.

38 M. Sasaki, Y. Kozukue, K. Hashimoto, K. Takayama, I. Nakamura, I. Takano and Y. Sawada, Properties of carbon films with a dose of titanium or zirconium prepared by magnetron sputtering, *Surf. Coat. Technol.*, 2005, **196**(1–3), 236–240.

39 S. Wei, H. Z. Hua and X. Xiang, Thermodynamic Analysis and Growth of Zirconium Carbide by Chemical Vapor Deposition, *Phys. Procedia*, 2013, **46**, 88–101.

40 Q. Meng, M. Wen, F. Mao, N. Nedfors, U. Jansson and W. Zheng, Deposition and characterization of reactive magnetron sputtered zirconium carbide films, *Surf. Coat. Technol.*, 2013, **232**, 876–883.

41 Y. Xin, S. Zhe-an, H. Qi-zhong, C. Li-yuan, Z. Ping and X. Liang, A zirconium carbide coating on graphite prepared by reactive melt infiltration, *J. Cent. South Univ. (Engl. Ed.)*, 2014, **21**, 472–476.

42 S. S. Kumar, A. Sharma, G. M. Rao and S. Suwas, Investigations on the effect of substrate temperature on the properties of reactively sputtered zirconium carbide thin films, *J. Alloys Compd.*, 2017, **695**, 1020–1028.

43 L. Yan, X. Zhang, P. Hu, G. Zhao, S. Dong, D. Liu and B. Sun, Carbon Nanofiber Arrays Grown on Three-Dimensional Carbon Fiber Architecture Substrate and Enhanced Interface Performance of Carbon Fiber and Zirconium Carbide Coating, *ACS Appl. Mater. Interfaces*, 2017, **9**, 17337–17946.

44 D. Craciun, G. Socol, N. Stefan, G. Bourne and V. Craciun, Chemical composition of ZrC thin films grown by pulsed laser deposition, *Appl. Surf. Sci.*, 2009, **255**(10), 5260–5263.

45 V. Craciun, E. McCumiskey, M. Hanna and C. Taylor, Very hard ZrC thin films grown by pulsed laser deposition, *J. Eur. Ceram. Soc.*, 2013, **33**, 2223–2226.

46 D. Craciun, G. Bourne, J. Zhang, K. Siebein, G. Socol, G. Dorcioman and V. Craciun, Thin and hard ZrC/TiN multilayers grown by pulsed laser deposition, *Surf. Coat. Technol.*, 2011, **205**, 5493–5496.

47 D. Craciun, G. Bourne, G. Socol, N. Stefan, G. Dorcioman, E. Lambers and V. Craciun, Characteristics of ZrC/ZrN and ZrC/TiN multilayers grown by pulse laser deposition, *Appl. Surf. Sci.*, 2011, **257**, 5332–5336.

48 S. N. L'vov, V. F. Nenchenko and G. V. Samsonov, Some characteristic features of the electrical properties of Groups IV–VI transition metal borides, carbides, and nitrides, *Dokl. Akad. Nauk SSSR*, 1960, **135**, 577.

49 E. K. Stromes, *MTP Int. Rev. Sci.: Inorg. Chem., Ser. One*, 1972, **10**, 37.

50 R. Keiffer and P. Ettmayer, *High Temperatures – High Pressures*, 1974, **6**, 253.

51 *Engineering property data on selected ceramics*, Nitrides, Batelle Colombus Laboratories, Ceramics Information Center, 1976, vol. 1, https://www.worldcat.org/title/engineering-property-data-on-selected-ceramics/oclc/22951037.

52 A. A. Zabolotskii, S. E. Salibekov, I. A. Kantsevich, N. P. Ignatova and A. I. Chernyak, Reaction between carbon fibers and nickel through a zirconium nitride or titanium carbide diffusion barrier, *Poroshk. Metall. (Kuibyshev)*, 1977, **7**(175), 32–35.

53 M. Caillet, H. F. Atedi and J. Besson, Etude de la corrosion de revetements refractaires sur le zirconium 1. Oxydation par l'oxygene de revetements de nitrure de zirconium, *J. Less-Common Met.*, 1977, **51**, 305–322.

54 R. G. Duckworth, High purity sputtered tribological coatings, *Thin Solid Films*, 1981, **86**(2–3), 213–218.

55 W. D. Sproul, Very high rate reactive sputtering of TiN, ZrN and HfN, *Thin Solid Films*, 1983, **107**, 141.

56 R. G. Duckworth, Sputtered coatings for metal finishing, *Trans. Inst. Met. Finish.*, 1984, **62**(1), 109–111.

57 R. G. Duckworth, Backscattering analysis of ZrN alloys, *Nucl. Instrum. Methods Phys. Res.*, 1986, **B15**, 272–274.

58 J. C. B. Simpson and L. G. Earwaker, Nuclear analysis of zirconium nitride thin films, *Nucl. Instrum. Methods Phys. Res.*, 1987, **B24/25**, 701–704.

59 A. Derradji and F. Kassabji, Preparation of plasma-sprayed coatings of ZrN under a controlled nitrogen atmosphere, *Surf. Coat. Technol.*, 1986, **29**, 291–301.

60 M. Valikhani and S. Chandrashekhar, Characteristics of TiN and ZrN Coatings on Split Point Drills Using the Static and Stochastic Models of the Force System as a Signature, *Int. J. Adv. Des. Manuf. Technol.*, 1987, **2**(1), 75–106.

61 J. A. Sue and H. H. Troue, Influence of crystallographic orientation, residual strains, crystallite size and microhardness on erosion in ZrN coating, *Surf. Coat. Technol.*, 1989, **39–40**(2), 421.

62 J. A. Sue and H. H. Troue, High temperature erosion behavior of titanium nitride and zirconium nitride coatings, *Surf. Coat. Technol.*, 1991, **49**, 31–39.

63 J. A. Sue and H. H. Trou, Zirconium nitride coated article and method for making same, CA 1302807C, 1992.

64 S. A. Muboyadzhyan, Erosion-Resistant Coatings for Gas Turbine Compressor Blades, *Russ. Metall.*, 2009, **2009**(3), 183–196.

65 J. Musil, I. Stepanek, J. J. Musil, M. Kolega, O. Blahova, J. Vyskocil and J. Kasl, Properties of TiN, ZrN and ZrTiN coatings prepared by cathodic arc evaporation, *Mater. Sci. Eng.*, 1993, **A163**, 211–214.

66 K. Gruss, T. Zheleva, R. Davis and T. Watkins, Characterization of zirconium nitride coatings deposited by cathodic arc sputtering, *Surf. Coat. Technol.*, 1998, **107**, 115–124.

67 J. Ramana, S. Kumar, C. David, A. Ray and V. Raju, Characterisation of zirconium nitride coatings prepared by DC magnetron sputtering, *Mater. Lett.*, 2000, **43**, 73–76.

68 J. Sue and T. Chang, Friction and wear behavior of titanium nitride, zirconium nitride and chromium nitride coatings at elevated temperatures, *Surf. Coat. Technol.*, 1995, **76–77**, 61–69.

69 J. A. Davidson, *Zirconium oxide and zirconium nitride coated biocompatible leads. Patent US005496359A*, 1996.

70 C.-H. Ma, J.-H. Huang and H. Chena, A study of preferred orientation of vanadium nitride and zirconium nitride coatings on silicon prepared by ion beam assisted deposition, *Surf. Coat. Technol.*, 2000, **133–134**, 289–294.

71 D. Pilloud, A. Dehlinger, J. Pierson, A. Roman and L. Pichon, Reactively sputtered zirconium nitride coatings: structural, mechanical, optical and electrical characteristics, *Surf. Coat. Technol.*, 2003, **174–175**, 338–344.

72 G. Lopez and M. Staia, High-temperature tribological characterization of zirconium nitride coatings, *Surf. Coat. Technol.*, 2005, **200**, 2092–2099.

73 E. A. Orlova, A. F. Gurbich, S. L. Molodtsov, V. V. Orlov, S. N. Bozin and A. V. Bashkin, Formation and investigation of nitride fuel compatible protective coatings on ferrite-martensite steel, *At. Energy*, 2008, **105**(5), 344–350.

74 M. Matsuoka, S. Isotani, W. Sucasaire, N. Kuratani and K. Ogata, X-ray photoelectron spectroscopy analysis of zirconium nitride-like films prepared on Si(100) substrates by ion beam assisted deposition, *Surf. Coat. Technol.*, 2008, **202**, 3129–3135.

75 Q. Meng, M. Wen, C. Qu, C. Hu and W. Zheng, Preferred orientation, phase transition and hardness for sputtered zirconium nitride films grown at different substrate biases, *Surf. Coat. Technol.*, 2011, **205**, 2865–2870.

76 S. A. Muboyadzhyan, Erosion-Resistant Metal Nitride Coatings and Carbide and Their Plasmochemical Synthesis, *Russ. J. Gen. Chem.*, 2011, **81**(5), 1053–1060.

77 D. Roman, J. Bernardi, C. L. D. Amorim, F. S. D. Souza, A. Spinelli, C. Giacomelli, C. A. Figueroa, I. J. Baumvol and R. L. Basso, Effect of deposition temperature on microstructure and corrosion resistance of ZrN thin films deposited by DC reactive magnetron sputtering, *Mater. Chem. Phys.*, 2011, **130**, 147–153.

78 A. Singh, N. Kumar, P. Kuppusami, T. Prasanthi, P. Chandramohan, S. Dash, M. Srinivasan, E. Mohandas and A. Tyagi, Tribological properties of sputter deposited ZrN coatings on titanium modified austenitic stainless steel, *Wear*, 2012, **280–281**, 22–27.

79 P. Klumdoung, A. Buranawong, S. Chaiyakun and P. Limsuwan, Variation of color in Zirconium nitride thin films prepared at high Ar flow rates with reactive dc magnetron sputtering, *Procedia Eng.*, 2012, **32**, 916–921.

80 A. Singh, P. Kuppusami, S. Khan, C. Sudha, R. Thirumurugesan, R. D. R. Ramaseshana and S. D. E. Mohandasb, Influence of nitrogen flow rate on microstructural and nanomechanical properties of Zr–N thin films prepared by pulsed DC magnetron sputtering, *Appl. Surf. Sci.*, 2013, **280**, 117–123.

81 T. Muneshwar and K. Cadien, Comparing XPS on bare and capped ZrN films grown by plasma enhanced ALD: effect of ambient oxidation, *Appl. Surf. Sci.*, 2018, **435**, 367–376.

82 C. D. S. Oliveira, D. Martinez-Martinez, L. Cunha, M. Rodrigues, J. Borges, C. Lopes, E. Alves, N. Barradas and M. Apreutesei, Zr-O-N coatings for decorative purposes: study of the system stability by exploration of the deposition parameter space, *Surf. Coat. Technol.*, 2018, **343**, 30–37.

83 D. Valerini, M. Signore, L. Tapfer, E. Piscopiello, U. Galietti and A. Rizzo, Adhesion and wear of ZrN films sputtered on tungsten carbide substrates, *Thin Solid Films*, 2013, **538**, 42–47.

84 Z. Qi, F. Zhu, Z. Wu, B. Liu, Z. Wang, D. Peng and C. Wu, Influence of yttrium addition on microstructure and mechanical properties of ZrN coatings, *Surf. Coat. Technol.*, 2013, **231**, 102–106.

85 F. Khatkhatay, J. Jian, L. Jiao, Q. Su, J. Gan, J. I. Cole and H. Wang, Diffusion barrier properties of nitride-based coatings on fuel cladding, *J. Alloys Compd.*, 2013, **580**, 442–448.

86 L. Sudderth, D. Perez-Nunez, D. Keiser and S. McDeavitt, Fabrication of ZrN Barrier Coatings for U-Mo Microspheres Via Fluidized Bed Chemical Vapor Deposition Using a Metalorganic Precursor, *Nucl. Technol.*, 2018, **202**, 81–93.

87 M. Rizzi, G. Gatti, M. Migliario, L. Marchese, V. Rocchetti and F. Renò, Effect of zirconium nitride physical vapor deposition coating on preosteoblast cell adhesion and proliferation onto titanium screws, *J. Prosthet. Dent.*, 2014, **112**(5), 1103–1110.

88 P. Prachar, S. Bartakova, V. Brezina, L. Cvrcek and J. Vanek, Cytocompatibility of implants coated with titanium nitride and zirconium nitride, *Bratisl. Lek. Listy*, 2015, **116**(3), 154–156, DOI: 10.4149/bll_2015_031.

89 M.-K. Ji, S.-W. Park, K. Lee, I.-C. Kang, K.-D. Yun and H.-S. Kim, Evaluation of antibacterial activity and osteoblast-like cell viability of TiN, ZrN and $(Ti_{1-x}Zr_x)N$ coating on titanium, *J. Adv. Prosthodont.*, 2015, **7**, 166–171.

90 G. Brunello, P. Brun, C. Gardin, L. Ferroni, E. Bressan, R. Meneghello, B. Zavan and S. Sivolella, Biocompatibility and antibacterial properties of zirconium nitride coating on titanium abutments: an *in vitro* study, *PLoS One*, 2018, **16**(6), 1–17.

91 A. L. P. Reyna, B. Fritz, J. Schwiesau, C. Schilling, B. Summer, P. Thomas and T. M. Grupp, Metal ion release barrier function and biotribological evaluation of a zirconium nitride multilayer coated knee implant under highly demanding activities wear simulation, *J. Biomech.*, 2018, **79**, 88–96.

92 M. Pilz, K. Staats, S. Tobudic, O. Assadian, E. Presterl, R. Windhager and J. Holinka, Zirconium Nitride Coating Reduced Staphylococcus epidermidis Biofilm Formation on Orthopaedic Implant Surfaces: An *In Vitro* Study, *Clin. Orthop. Relat. Res.*, 2019, **477**(2), 461–466.

93 S. Khan, M. Mehmood, I. Ahmad, F. Ali and A. Shah, Structural and electrical resistivity characteristics of vacuum arc ion deposited zirconium nitride thin films, *Mater. Sci. Semicond. Process.*, 2015, **30**, 486–493.

94 P. Patsalas, N. Kalfagiannis, S. Kassavetis, G. Abadias, D. Bellas, C. Lekka and E. Lidorikis, Conductive nitrides: growth principles, optical and electronic properties, and their perspectives in photonics and plasmonics, *Mater. Sci. Eng., R*, 2018, **123**, 1–55.

95 J.-P. Meng, Z.-Q. Fu, M. Du, X.-P. Liu and L. Hao, Influence of ion-atom arrival ratio on structure and optical properties of ZrNx films, *Mater. Lett.*, 2016, **164**, 291–293.

96 C. Martin, K. Miller, H. Makino, D. Craciun, D. Simeone and V. Craciun, Optical properties of Ar ions irradiated nanocrystalline ZrC and ZrN thin films, *J. Nucl. Mater.*, 2017, **488**, 16–21.

97 Z. Gao, Y. Chen, J. Kulczyk-Malecka, P. Kelly, Y. Zeng, X. Zhang, H. L. Chun Li, N. Rohbeck and P. Xiao, Comparison of the oxidation behavior of a zirconium nitride coating in water vapor and air at high temperature, *Corros. Sci.*, 2018, **138**, 242–251.

98 M. Jean, C. Liu, S. Chiu and T. H. Chien, Modelling, Fabrication and Optimization for Hard Coatings of Deposited Ceramic Nitride Films Using a Magnetron Sputtering, *Phys. Procedia*, 2012, **32**, 289–296.

99 J. M. Kapopara, A. R. Mengarb, K. V. Chauhan and S. K. Rawal, CFD Analysis of Sputtered TiN Coating, *Mater. Today*, 2017, **4**, 9390–9393.

100 J. M. Kapopara, N. P. Patel, D. J. Kotadiya, A. R. Patel, K. V. Chauhan and S. K. Rawal, FEA Analysis of Zirconium Nitride Coatings Prepared by RF Magnetron Sputtering: CFD Approach, *Mater. Today: Proc.*, 2018, **5**, 5338–5342.

101 I. T. S. A. L. V. Kbzlovskii, Mechanical properties and corrosion resistance of steels with titanium and zirconium carbonitride coatings, *Prot. Met.*, 1970, **6**(5), 567–570.

102 M. Caillet and H. F. A. A. J. Besson, Etude de la corrosion de revetements refractaires sur le zirconium III. Oxydation pr la vapeur deau de revetements de nitrure et de carbonitrure de zirconium, *J. Less-Common Met.*, 1978, **58**, 37–46.

103 H. Berndt, A.-Q. Zeng, H.-R. Stock and P. May, Zirconium carbonitride films produced by plasma-assisted metal organic chemical vapour deposition, *Surf. Coat. Technol.*, 1995, **74–75**, 369–374.

104 E. Grigore, C. Ruset, X. Li and H. Dong, Zirconium carbonitride films deposited by combined magnetron sputtering and ion implantation (CMSII), *Surf. Coat. Technol.*, 2010, **204**, 1889–1892.

105 A. Cavaleiro, S. Calderon V and S. Carvalho, Chemical and structural characterization of Zr C N Ag coatings: XPS, XRD and Raman spectroscopy, *Appl. Surf. Sci.*, 2015, **346**, 240–247.

106 B. Usmani, V. Vijay, R. Chhibber and A. Dixit, Effect of Growth Condition on Mechanical Properties of Zirconium Carbonitride Absorber-Based Spectrally Selective Coatings, in *Concentrated Solar Thermal Energy Technologies*, ed. L. Chandra and A. Dixit, 2018, pp. 137–143.

107 S. Calderon V, R. E. Galindo, J. Oliveira, A. Cavaleiro and S. Carvalho, Ag^+ release and corrosion behavior of zirconium carbonitride coatings with silver nanoparticles for biomedical devices, *Surf. Coat. Technol.*, 2013, **222**, 104–111.

108 S. Calderon V, J. Oliveira, M. Evaristo, A. Cavaleiro and S. Carvalho, Prediction of optimized composition for enhanced mechanical and electrochemical response of Zr–C–N–Ag coatings for medical devices S, *Appl. Surf. Sci.*, 2014, **320**, 570–580.

109 I. Ferreri, V. Lopes, S. Calderon V, C. Tavares, A. Cavaleiro and S. Carvalho, Study of the effect of the silver content on the structural and mechanical behavior of Ag–ZrCN coatings for orthopedic prostheses, *Mater. Sci. Eng., C*, 2014, **42**, 782–790.

110 L. Wang, X. Zhao, M. Ding, H. Zheng, H. Zhang, B. Zhang, X. Li and G. Wu, Surface modification of biomedical AISI 316L stainless steel with zirconium carbonitride coatings, *Appl. Surf. Sci.*, 2015, **340**, 113–119.

111 I. Ferreri, S. Calderon V, R. E. Galindo, C. Palacio, M. Henriques, A. Piedade and S. Carvalho, Silver activation on thin films of Ag–ZrCN coatings for antimicrobial activity, *Mater. Sci. Eng., C*, 2015, **55**, 547–555.

112 S. Calderon V, A. Cavaleiro and S. Carvalhoa, Electrochemical response of ZrCN-Ag-a(C,N) coatings in simulated body fluids, *Electrochim. Acta*, 2015, **176**, 898–906.

113 S. Calderon V, I. Ferreri, M. Henriques, J. DeHosson, A. Cavaleiro and S. Carvalho, Nano-galvanic coupling for enhanced Ag^+ release in ZrCN–Ag films: antibacterial application, *Surf. Coat. Technol.*, 2016, **298**, 1–6.

114 S.-H. Yao, Y.-L. Su and Y.-C. Lai, Antibacterial and Tribological Performance of Carbonitride Coatings Doped with W, Ti, Zr, or Cr Deposited on AISI 316L Stainless Steel, *Materials*, 2017, **10**, 1189.

115 C.-H. Lai, M.-H. Tsai, S.-J. Lin and J.-W. Yeh, Influence of substrate temperature on structure and mechanical, properties of multi-element (AlCrTaTiZr)N coatings, *Surf. Coat. Technol.*, 2007, **201**(16–17), 6993–6998.

116 P. Dubey, V. Arya, S. Srivastava, D. Singh and R. Chandra, Effect of nitrogen flow rate on structural and mechanical properties of Zirconium Tungsten Nitride (Zr–W–N) coatings deposited by magnetron sputtering, *Surf. Coat. Technol.*, 2013, **236**, 182–187.

117 E. Silva, M. R. D. Figueiredo, R. Franz, R. E. Galindo, C. Palacio, A. Espinosa, S. Calderon V, C. Mitterer and S. Carvalho, Structure–property relations in ZrCN coatings for tribological applications, *Surf. Coat. Technol.*, 2010, **205**(7), 2134–2141.

118 M. Braic, M. Balaceanu, A. Vladescu, C. N. Zoita and V. Braic, Study of (Zr,Ti)CN, (Zr,Hf)CN and (Zr,Nb)CN films prepared by reactive magnetron sputtering, *Thin Solid Films*, 2011, **519**(12), 4092–4096.

119 G. Abadias, L. E. Koutsokeras, P. Guerin and P. Patsalas, Stress evolution in magnetron sputtered Ti–Zr–N and Ti–Ta–N films studied by *in situ* wafer curvature: role of energetic particles, *Thin Solid Films*, 2009, **518**(5), 1532–1537.

120 M. Balaceanu, T. Petreus, V. Braic, C. N. Zoita, A. Vladescu, C. E. Cotrutz and M. Braic, Characterization of Zr-based hard coatings for medical implant applications, *Surf. Coat. Technol.*, 2010, **204**(12–13), 2046–2050.

121 M. M. Larijani, M. B. Zanjanbar and A. Majdabadi, The effect of carbon fraction in Zr(C, N) films on the nanostructural properties and hardness, *J. Alloys Compd.*, 2010, **492**(1–2), 735–738.

122 G. Abadias, F. Pailloux and S. N. Dub, Epitaxial growth and mechanical properties of (001) ZrN/W nanolaminates, *Surf. Coat. Technol.*, 2008, **202**(15), 3683–3687.

123 M. Braic, V. Braic, M. Balaceanu, C. N. Zoita, A. Kiss, A. Vladescu, A. Popescu and R. Ripeanu, M. Braic, V. Braic, M. Balaceanu, C. N. Zoita, A. Kiss, A. Structure and properties of Zr/ZrCN coatings deposited by cathodic arc method, *Mater. Chem. Phys.*, 2011, **126**(3), 818–825.

124 F. Hollstein, D. Kitta, P. Louda, F. Pacal and J. Meinhardt, F. Hollstein, Investigation of low-reflective ZrCN PVD-arc coatings for application on medical tools for minimally invasive surgery, *Surf. Coat. Technol.*, 2001, **142–144**, 1063–1068.

125 S.-F. Chen, Y.-C. Kuo, C.-J. Wang, S.-H. Huang, J.-W. Lee, Y.-C. Chan, H.-W. Chen, J.-G. Duh and T.-E. Hsieh, The effect of Cr/Zr chemical composition ratios on the mechanical properties of CrN/ZrN multilayered coatings deposited by cathodic arc deposition system, *Surf. Coat. Technol.*, 2013, **231**, 247–252.

126 Y.-Y. Chang and C.-J. Wu, Mechanical properties and impact resistance of multilayered TiAlN/ZrN coatings, *Surf. Coat. Technol.*, 2013, **231**, 62–66.

127 C.-H. Lai, Y.-Y. Chang, H.-L. Huang and H.-Y. Kao, Characterization and antibacterial performance of ZrCN/amorphous carbon coatings deposited on titanium implants, *Thin Solid Films*, 2011, **520**(5), 1525–1531.

128 M. Braic, M. Balaceanu, A. Vladescu, A. Kiss, V. Braic, A. Purice, G. Dinescu, N. Scarisoreanu, F. Stokker-Cheregi, A. Moldovan, R. Birjega and M. Dinescu, TiN/ZrN heterostructures deposition and characterisation, *Surf. Coat. Technol.*, 2006, **200**(22–23), 6505–6510.

129 D. Craciun, G. Socol, G. Dorcioman, N. Stefan, G. Bourne and V. Craciun, High quality ZrC, ZrC/ZrN and ZrC/TiN thin films grown by pulsed laser deposition, *J. Optoelectron. Adv. Mater.*, 2010, **12**(3), 461–465.

130 Y. Long, A. Javed, J. Chen, Z. Chen and X. Xiong, Phase composition, microstructure and mechanical properties of ZrC coatings produced by chemical vapor deposition, *Ceram. Int.*, 2014, **40**(1), 707–713.

131 S. Kudapa, K. Narasimhan, P. Boppana and W. C. Russell, Characterization and properties of MTCVD TiCN and MTCVD ZrCN coatings, *Surf. Coat. Technol.*, 1999, **120–121**, 259–264.

132 K. Rie, A. Gebauer and J. Wohle, Plasma assisted CVD for low temperature coatings to improve the wear and corrosion resistance, *Surf. Coat. Technol.*, 1996, **87**, 498–506.

133 J. Wohle, C. Pfohl, K. Rie, A. Gebauer-teichmann and S. K. Kim, Deposition of TiCN and ZrCN layers on light metals by PACVD method using radio frequency and pulsed-DC plasma, *Surf. Coat. Technol.*, 2000, **131**, 127–130.

134 S.-L. Wang, K.-Z. Li, H.-J. Li, Y.-L. Zhang and Y.-J. Wang, Effects of microstructures on the ablation behaviors of ZrC deposited by CVD, *Surf. Coat. Technol.*, 2014, **240**, 450–455.

135 V. Braic, M. Braic, M. Balaceanu, A. Vladescu, C. N. Zoita, I. Titorencu and V. Jinga, (Zr,Ti)CN coatings as potential candidates for biomedical applications, *Surf. Coat. Technol.*, 2011, **206**(4), 604–609.

136 L. F. Senna, C. A. Achete, F. L. Freire JR. and T. Hirsch, The effect of deposition parameters on the chemical composition and corrosion resistance of TiC_xN_y coatings produced on high-speed steel substrates, *Braz. J. Chem. Eng.*, 2001, **18**(4), 399–409.

137 K. Rie and J. Wohle, Plasma-CVD of TiCN and ZrCN films on light metals, *Surf. Coat. Technol.*, 1999, **112**, 226–229.

138 W. Ensinger, A. Schroer and G. K. Wolf, A comparison of IBAD films for wear and corrosion protection with other PVD coatings, *Nucl. Instrum. Methods Phys. Res., Sect. B*, 1993, **80–81**, 445.

139 L. Fedrizzi, M. Elena, S. Gialanella, M. Dapor and L. Guzman, *Mater. Sci. Eng., A*, 1989, **116**, 47.

140 L. Guzman and M. Elena, *Mater. Sci. Forum*, 1990, **54–55**, 21.

141 X.-Y. Wen and Z. Zhang, *Surf. Coat. Technol.*, 1992, **51**, 252.

142 A. Kluge, B. H.-S. Javadi, H. Ruoff, R. Öchsner and H. Ryssel, *Surf. Coat. Technol.*, 1992, **51**, 237.

143 K. Bouslykhane, J. V. P. Moine and J. Grilhe, *Surf. Coat. Technol.*, 1991, **49**, 457.

144 I. Khan, S. Jabbar, T. Hussain, M. Hassan, R. Ahmad, M. Zakaullah and R. Rawat, Deposition of zirconium carbonitride composite films using ion and electron beams emitted from plasma focus device, *Nucl. Instrum. Methods Phys. Res., Sect. B*, 2010, **268**, 2228–2234.

145 L. Pichon, T. Girardeau, A. Straboni, F. Lignou, J. Perriere and J. Frigerio, Ion beam assisted deposition of zirconium nitrides for modulated optical index structures, *Nucl. Instrum. Methods Phys. Res., Sect. B*, 1999, **147**, 378–382.

146 C.-P. Liu and H.-G. Yang, Systematic study of the evolution of texture and electrical properties of ZrN x thin films by reactive DC magnetron sputtering, *Thin Solid Films*, 2003, **444**, 111.

147 M. Yoshitake, T. Yotsuya and S. Ogawa, Effects of Nitrogen Pressure and RF Power on the Properties of Reactive Magnetron Sputtered Zr–N Films and an Application to a Thermistor, *Jpn. J. Appl. Phys.*, 1992, **31 Part 1**(12A), 4002.

148 N. Farkas, G. Zhang, R. Ramsier, E. Evans and J. Dagata, Characterization of zirconium nitride films sputter

deposited with an extensive range of nitrogen flow rates, *J. Vac. Sci. Technol., A*, 2008, **26**, 297.

149 S. Camelio, T. Girardeau, L. Pichon, A. Straboni, C. Fayoux and P. Guérin, Transformation of the semi-transparent into the metallic phase of zirconium nitride compounds by implantation at controlled temperature: the evolution of the optical properties, *J. Opt. A: Pure Appl. Opt.*, 2000, **2**(5), 442–448.

150 M. Nose, M. Zhou, E. Honbo, M. Yokota and S. Saji, Colorimetric properties of ZrN and TiN coatings prepared by DC reactive sputtering, *Surf. Coat. Technol.*, 2001, **142–144**, 211–217.

151 H. M. Benia, M. Guemmaz, G. Schmerber, A. Mosser and J.-C. Parlebas, *Appl. Surf. Sci.*, 2002, **200**, 231.

152 R. Lamni, E. Martinez, S. G. Springer, R. Sanjinés, P. E. Schmid and F. Lévy, *Thin Solid Films*, 2004, **447–448**, 316.

153 J.-H. Huang, C.-H. Ho and Y. Ge-Ping, Effect of Nitrogen Flow Rate on the Structure and Mechanical Properties of ZrN Thin Film on Si(100) and Stainless Steel Substrates, *Mater. Chem. Phys.*, 2007, **102**, 31–38.

154 A. Johansen, J. H. Dontje and R. L. D. Zenner, Reactive arc vapor ion deposition of TiN, ZrN and HfN, *Thin Solid Films*, 1987, **153**, 75–82.

155 J. P. Zhao, X. Wang, Z. Y. Chen, S. Q. Yang, T. S. Shi and X. H. Liu, Overall energy model for preferred growth of TiN films during filtered arc deposition, *J. Phys. D: Appl. Phys.*, 1997, **30**, 5–12.

156 R. Manaila, D. Biro, A. Devenyi, D. Fratiloiu, R. Popescu and J. E. Totolici, Structure of nitride film hard coatings prepared by reactive magnetron sputtering, *Appl. Surf. Sci.*, 1998, **134**, 1–10.

157 H. Benia, M. Guemmaz, G. Schmerber, A. Mosser and J. C. Parlebas, Investigations on non-stiochiometric zirconium nitrides, *Appl. Surf. Sci.*, 2002, **200**, 231–238.

158 S. Binder, W. Lengauer, P. Ettmayer, J. Bauer, J. Debuigne and M. Bohn, Phase equilibria in the systems Ti–C–N, Zr–C–N and Hf–C–N, *J. Alloys Compd.*, 1995, **217**(1), 128–136.

159 X.-M. He, L. Shu, H.-B. Li and H.-D. Li, Structural characteristics and hardness of zirconium carbide films prepared by tri-ion beam-assisted deposition, *J. Vac. Sci. Technol., A*, 1998, **16**(4), 2337.

160 M. Balaceanu, V. Braic, A. Kiss, C. N. Zoita, A. Vladescu, M. Braic, I. Tudor, A. Popescu, R. Ripeanu, C. Logofatu and C. C. Negrila, Characteristics of arc plasma deposited TiAlZrCN coatings, *Surf. Coat. Technol.*, 2008, **202**(16), 3981–3987.

161 Z. Qi, P. Sun, F. Zhu, Z. Wang, D. Peng and C. Wu, *Surf. Coat. Technol.*, 2011, **205**, 3692.

162 J. Li, *Trans. Metall. Soc. AIME*, 1963, **227**, 239.

163 S. Yao, Y. Su, W. Kao and K. Cheng, Wear behavior of DC unbalanced magnetron sputter deposited ZrCN films, *Mater. Lett.*, 2005, **59**, 3230.

164 Q. Yang, W. Lengauer, T. Koch, M. Scheerer and I. Smid, *J. Alloys Compd.*, 2000, **L5–L9**, 309.

165 H.-M. Tung, J.-H. Huang, D.-G. Tsai, C.-F. Ai and Y. Ge-Ping, Hardness and residual stress in nanocrystalline ZrN films: effect of bias voltage and heat treatment, *Mater. Sci. Eng., A*, 2009, **500**(1–2), 104–108.

166 G. Abadias, Y. Tse and P. Guerin, Interdependence between stress, preferred orientation, and surface morphology of nanocrystalline TiN thin films deposited by dual ion beam sputtering, *J. Appl. Phys.*, 2006, **99**, 113519.

167 J.-H. Huang, C.-Y. Hsu, S.-S. Chen and G.-P. Yu, Effect of substrate bias on the structure and properties of ion-plated ZrN on Si and stainless steel substrates, *Mater. Chem. Phys.*, 2002, **77**, 14–21.

168 W. Ensinger, K. Volz and M. Kiuchi, Ion beam-assisted deposition of nitrides of the 4th group of transition metals, *Surf. Coat. Technol.*, 2000, **128–129**, 81.

169 W. Ensinger, *Nucl. Instrum. Methods Phys. Res., Sect. B*, 1997, **127–128**, 796.

170 W.-J. Chou, G.-P. Yu and J.-H. Huang, Bias effect of ion-plated zirconium nitride film on Si(100), *Thin Solid Films*, 2002, **405**, 162–169.

171 Z. Wokulski, *Phys. Status Solidi A*, 1990, **120**, 175.

172 S. Khan, M. Mehmood, I. Ahmad, F. Ali and A. Shah, Structural and electrical resistivity characteristics of vacuum arc ion deposited zirconium nitride thin films, *Mater. Sci. Semicond. Process.*, 2015, **30**, 486–493.

173 E. W. Niu, L. Li, G. H. Lv, H. Chen, W. R. Feng, S. H. Fan, S. Z. Yang and X. Z. Yang, *Mater. Sci. Eng., A*, 2007, **460–461**, 135–139.

174 S. Horita, M. Kobayashi, H. Akahori and T. Hata, Material properties of ZrN film on silicon prepared by low-energy ion-assisted deposition, *Surf. Coat. Technol.*, 1994, **66**, 318–323.